Contrib Mineral Petrol (2003) 145: 281–300
DOI 10.1007/s00410-003-0452-3

ORIGINAL PAPER

Michael Bizimis · Vincent J. M. Salters
J. Barry Dawson

The brevity of carbonatite sources in the mantle: evidence from Hf isotopes

Received: 14 June 2002 / Accepted: 15 December 2002 / Published online: 3 April 2003

Abstract Hf, Zr and Ti in carbonatites primarily reside in their non-carbonate fraction while the carbonate fraction dominates the Nd and Sr elemental budget of the whole rock. A detailed investigation of the Hf, Nd and Sr isotopic compositions shows frequent isotopic disequilibrium between the carbonate and non-carbonate fractions. We suggest that the trace element and isotopic composition of the carbonate fraction better represents that of the carbonatite magma, which in turn better reflects the composition of the carbonatitic source. Experimental partitioning data between carbonatite melt and peridotitic mineralogy suggest that the Lu/Hf ratio of the carbonatite source will be equal to or greater than the Lu/Hf ratio of the carbonatite. This, combined with the Hf isotope systematics of carbonatites, suggests that, if carbonatites are primary mantle melts, then their sources must be short-lived features in the mantle (maximum age of 10–30 Ma), otherwise they would develop extremely radiogenic Hf compositions. Alternatively, if carbonatites are products of extreme crystal fractionation or liquid immiscibility then the lack of radiogenic initial Hf isotope compositions also suggests that their sources do not have long-lived Hf depletions. We present a model in which the carbonatite source is created in the sublithospheric mantle by the crystallization of earlier carbonatitic melts from a mantle plume. This new source melts shortly after its formation by the excess heat provided by the approaching hotter center of the plume and/or the subsequent ascending silicate melts. This model explains the HIMU-EMI isotope characteristics of the East African carbonatites, their high LREE/HREE ratios as well as the rarity of carbonatites in the oceanic lithosphere.

M. Bizimis (✉) · V. J. M. Salters
National High Magnetic Field Laboratory
and Department of Geological Sciences,
Florida State University, 1800 E. Paul Dirac Drive,
Tallahassee, FL, 32306, USA
E-mail: bizimis@magnet.fsu.edu
Tel.: -+1-850-6442263
Fax: +1-850-6440827

J. B. Dawson
Department of Geology and Geophysics,
University of Edinburgh, West Mains Road,
EH9 3JW, Edinburgh, Scotland

M. Bizimis
Department of Earth Sciences,
Florida International University, Miami, FL, 33199, USA

Editorial responsibility: T.L. Grove

Introduction

Carbonatites are magmatic, carbonate-rich rocks closely associated with alkaline igneous complexes. At least half of the known carbonatite complexes occur in Africa and most of them are associated with the East African rift (Woolley 1989, 2001). Carbonatites are characterized by very high light rare earth (LREE) and other trace element contents (e.g. Ba, Sr, Nb, Th, U), large Hf, Zr and Ti depletions and high Lu/Hf ratios (Nelson et al. 1988; Woolley and Kempe 1989). Their elevated Sr and Nd contents suggests that their Sr and Nd isotope ratios cannot be significantly modified by crustal contamination and as such, their Nd and Sr isotopic compositions are believed to closely reflect that of their sources (e.g. Bell and Blenkinsop, 1987). The generally radiogenic Nd and unradiogenic Sr isotopic compositions of carbonatites suggest derivation from a long-term depleted mantle reservoir (Bell 1998; Bell and Blenkinsop 1987; Harmer and Gittins 1998; Nelson et al. 1988). Recent studies on the East African carbonatites suggest that their Nd, Sr and Pb isotopic compositions are consistent with mixing between HIMU and EMI mantle components, which are either part of an isotopically heterogeneous mantle plume (Bell 1998; Bell and Tilton 2001), or products of a old heterogeneous lithospheric mantle source produced by variable depletion and enrichment events (Kalt et al. 1997).

Carbonatites are also frequently invoked as metasomatizing agents in the mantle and several suites of

peridotites show features compatible with carbonatitic metasomatism (Coltorti et al. 1999; Dawson 1987; Hauri et al. 1993; Rudnick et al. 1993; Yaxley et al. 1991, 1998). However, carbonate phases in peridotite xenoliths (e.g. Dawson et al. 1970; Ionov 1998; Lee et al. 2000; Ionov and Harmer, 2002) generally have lower trace element contents and more restricted major element compositions than the erupted carbonatites. Thus, Lee and Wyllie (1997a), Lee et al. (2000) and Ionov and Harmer (2002) interpreted these carbonates as cumulates from a carbonatitic magma, rather than a source for carbonatites.

Carbonatites are believed to represent either primary melts from the mantle, or products of liquid immiscibility/crystal fractionation (further discussed later). The available peridotite–mineral/carbonatite–melt partition coefficients are similar for Lu and Hf (e.g. Adam and Green 2001; Green et al. 1992), suggesting limited Lu/Hf fractionation between source and carbonatite during melting. Therefore, if carbonatites represent primary mantle melts then their high Lu/Hf ratios should reflect that of their sources. Such sources will then develop highly radiogenic Hf isotopic compositions if they existed in the mantle (or crust) for a significant period of time (> 100 Ma). However, the robust slope of the terrestrial array in Nd/Hf isotope space (Salters and White 1998; Vervoort et al. 1999) suggests that the long-term relative fractionation of the Sm/Nd and Lu/Hf isotopic systems has remained relatively constant in terrestrial reservoirs, with no obvious contribution from a long-lived carbonatite source. Here, we present a detailed Hf, Nd, Sr and Pb isotope and trace element investigation of carbonatites from East Africa, South Africa and Canada, in order to constrain the longevity and origin of the carbonatite sources in the mantle and their potential in decoupling the Nd/Hf isotopic system in terrestrial magmas.

Whole rock characteristics

The carbonatite samples from this study are from young (< 130 Ma) volcanics associated with the East African Rift and the Canadian Craton and from Proterozoic complexes from the South African craton. Sample descriptions, location and ages are presented in Table 1. Analytical techniques for the trace element and isotope determinations are presented in the Appendix.

Trace element concentrations

The whole rock trace element concentrations are reported in Table 2 and the REE and trace element patterns are plotted in Figs. 1 and 2. Characteristic features of all samples are the steep and variable LREE/HREE slopes (La_n/Lu_n 9–7561, n = chondrite-normalized) and the high absolute contents of Ba, Th, U, Nb, Ta, Sr and LREE. The chondrite-normalized REE patterns are

Table 1 Sample location, ages, major and minor mineral phases and references

Sample	Locality	Age (Ma)	Mineralogy: major/minor	References
BD 114	Oldoinyo Lengai, Tanzania	0	Nyerereite, gregoryite/sulfide, sylvite	Dawson et al. (1995); Simonetti et al. (1997)
BD 724	Museum Zone, Panda Hill, Tanzania	113 ± 6	Calcite/apatite, magnetite pyrochlore	Dawson et al. (1996); Van Straaten (1989)
BD 1476	Bukusu, Uganda	40 (25–55)	Calcite/magnetite, phlogopite, apatite	Dawson (unpubl.)
				Bell and Blenkinsop (1987); Nelson et al. (1988)
BD 1488	Sukulu, Uganda	40 (25–55)	Calcite, dolomite/magnetite, apatite, zircon, pyrochlore	Nelson et al. (1988); Dawson et al. (1996)
BD 1584	Central zone Chilwa Island, S.Malawi	130	Ankerite/apatite pyrochlore, magnetite	Simonetti and Bell (1994)
BD 1550	Kangankunde, S. Malawi	126	Calcite/magnetite, apatite	Nelson et al. (1988)
BD 1577	Nathace Hill, Tundulu, S. Malawi	130[a]	Bastnaesite-ankerite/apatite, magnetite	Garson (1962)
BD 1261	Deerdepoort, Pretoria	1,340[a]	Ankerite, calcite/K-feldspar, magnetite, apatite, quartz	Verwoerd (1967)
BD 1309	Central plug, Spitzkop, S. Africa	1,340	Calcite/apatite, phlogopite	Harmer (1999);Verwoerd (1967)
BD 1290	Central plug, Nooitgedacht, W. Transvaal	1,269	Calcite, ankerite/apatite, quartz	Verwoerd (1967)
A-12	Bond Zone, Oka complex, Canada	109	Calcite/niocalite, magnetite	Grünenfelderet al. (1986); Wen et al. (1987)
COQ	Oka complex, Canada	109	Carbonatite	USGS, reference material

[a]Age for sample BD 1577 is assumed at 130 Ma, similar to the BD 1584 also from S. Malawi. BD 1261 age is assumed at 1.34 Ga similar to the ages of other South African carbonatites (Harmer 1985)

Table 2 Whole rock trace element concentration in carbonatites (ppm)

	BD724	BD114	BD1476	BD1488	BD1584	BD1577	A12	BD1309	BD1290	BD1261	COQ	Average carbonatite
Rb	0.27	188.1	0.80	1.06	0.10	1.13	0.53	0.11	0.44	0.06	13.34	18.72
Sr	6159	10366	3531	3584	3204	45737	13281	1732	7941	3648	11781	10088
Y	92.82	4.30	58.12	56.33	143.9	25.32	96.86	232.7	70.08	109.6	100.5	90.06
Zr	27.79	0.46	10.81	28.56	80.66	2.12	176.77	9.16	12.51	319.4	77.02	67.76
Nb	827.2	14.34	189.9	23.34	70.75	262.3	11411	16.06	215.6	15.72	1739	1344
Ba	507.4	3835	473.6	340.0	4990	16119	970.2	97.5	225.8	240.3	1110	2628
La	359.7	439.5	209.1	141.5	1785	12023	1668	188.7	200.5	457.5	857.5	1666
Ce	709.7	451.8	368.1	290.7	3087	13381	3002	439.8	488.1	790.3	1744	2250
Pr	76.4	30.9	40.5	35.6	308.0	966.1	292.2	59.5	56.9	79.2	150.3	190.5
Nd	274.9	71.4	147.7	140.9	967.2	2.206	887.7	256.9	218.9	244.0	472.4	535.4
Sm	40.1	4.4	24.3	24.8	117.3	136.3	88.0	53.1	35.1	31.5	54.1	55.3
Eu	10.52	0.82	6.84	6.92	28.18	24.31	19.87	16.14	9.38	8.01	14.12	13.19
Gd	27.72	1.78	18.86	19.80	66.08	45.99	41.21	49.24	24.11	21.61	29.88	31.48
Tb	3.52	0.14	2.45	2.49	7.35	3.16	4.26	7.20	2.99	3.02	3.81	3.67
Dy	17.35	0.51	11.85	11.94	30.46	8.93	18.17	40.91	13.95	16.88	18.38	17.21
Ho	3.08	0.07	2.04	2.04	4.59	0.99	2.94	8.26	2.30	3.31	3.25	2.99
Er	7.63	0.15	4.77	4.74	9.81	1.69	7.08	22.25	5.17	8.47	8.21	7.27
Yb	6.17	0.10	3.22	3.07	6.72	1.06	5.84	16.23	3.26	5.59	6.33	5.24
Lu	0.90	0.02	0.45	0.43	0.94	0.16	0.87	2.07	0.43	0.67	0.86	0.71
Hf	0.49	0.01	0.40	0.69	0.95	0.06	0.38	0.27	0.17	3.00	0.28	0.61
Ta	2.23	0.06	83.31	1.30	0.30	0.04	430.4	2.27	1.40	0.34	25.99	49.79
Pb	12.85	61.04	4.87	3.34	90.74	88.55	2.10	11.99	6.17	16.42	4.13	27.47
Th	133.8	1.69	5.02	3.03	205.8	185.5	9.65	3.52	17.96	19.12	11.53	54.25
U	2.83	5.91	50.11	0.96	1.60	1.63	52.95	2.11	2.56	1.81	11.30	12.16
Sc	2.89	0.02	5.06	9.64	6.69	3.18	0.58	1.73	6.73	3.54	0.91	3.72
Ti	197.7	41.35	31.53	166.3	565.7	71.81	978.1	514.7	59.49	36.19	897.4	323.6
V	11.95	173.2	3.48	47.01	74.75	33.88	140.1	23.40	29.30	42.85	140.1	65.46
Hf/Hf*	0.0189	0.0025	0.0273	0.0488	0.0109	0.0003	0.0049	0.0099	0.0080	0.1335	0.0064	0.0128
Zr/Zr*	0.016	0.001	0.012	0.032	0.014	0.0002	0.033	0.006	0.009	0.215	0.027	0.021
Ti/Ti*	0.0027	0.0080	0.0007	0.0034	0.0031	0.0005	0.0079	0.0043	0.001	0.0007	0.0102	0.0038

steep in the LREE to MREE range and tend to flatten out towards the HREE. The two samples with the highest and lowest total REE contents (Nathace Hill, Oldoinyo Lengai) have the most fractionated REE patterns, similar to other Oldoinyo Lengai data (Simonetti et al. 1997). A prominent feature of all samples is their large and variable Hf, Zr and Ti depletions relative to the adjacent REE in an extended trace element diagram (Hf/Hf*, Zr/Zr*, Ti/Ti*, see Appendix for definition of these ratios), with the Ti depletions being generally greater than the Zr or Hf depletions (Table 2, Fig. 2). The Zr/Hf ratios range from 27 to 470 (average Zr/Hf = 113), with most being higher than chondritic (Zr/Hf = 36). This observation agrees with earlier studies suggesting that high Zr/Hf ratios are indicative of carbonatitic metasomatism (Dupuy et al. 1992), but based on the trace element patterns of carbonatites (Fig. 2), the Hf/Hf*, Zr/Zr* and Ti/Ti* ratios should be more robust indicators of carbonatite metasomatism. Such depletions are frequently observed in mantle xenoliths (e.g. Hauri et al. 1993; Ionov 1998; Rudnick et al. 1993; Salters and Shimizu 1988; Yaxley et al. 1998) and can sometimes be explained by carbonatitic metasomatism. The calculated average carbonatite trace element composition from these samples (Table 2, Fig. 3) is similar to the average calcio-carbonatite of Woolley and Kempe (1989). Our larger data-set for certain elements including Lu and Hf, relative to the Woolley and Kempe (1989) average and the higher precision of the ICP-MS technique, makes this a more robust estimate of an average carbonatite. As noted by Woolley and Kempe (1989) and Harmer (1999), care should be taken when using such an average composition because of the extreme ranges observed in certain elements in carbonatites (e.g. Nb, Sr, Ba). Nevertheless, certain important characteristics of carbonatites are evident from both averages, namely the large Hf, Zr and Ti depletions, the high Nb, Ba, Th and U contents and the high LREE/HREE ratios. Although the major element differences between different types of carbonatites (calcio-magnesio-ferro- carbonatites) are not considered here, this "grand" average can be especially useful for geochemical modeling where the trace element composition of an average carbonatite is required.

Nd, Sr and Pb isotope compositions

The whole rock Nd and Sr isotopic compositions of these samples are presented in Table 3 and plotted in Fig. 4. On a Nd/Sr isotope correlation plot, all samples fall close to or within the range of previously published data from these complexes (see Fig. 4 caption for references). The Ugandan samples (Bukusu and Sukulu) fall close to the HIMU mantle end member, while the zero age carbonatite from Oldoinyo Lengai falls close to the Bulk Earth value. The samples from Malawi form a horizontal field internal to the MORB-OIB array with

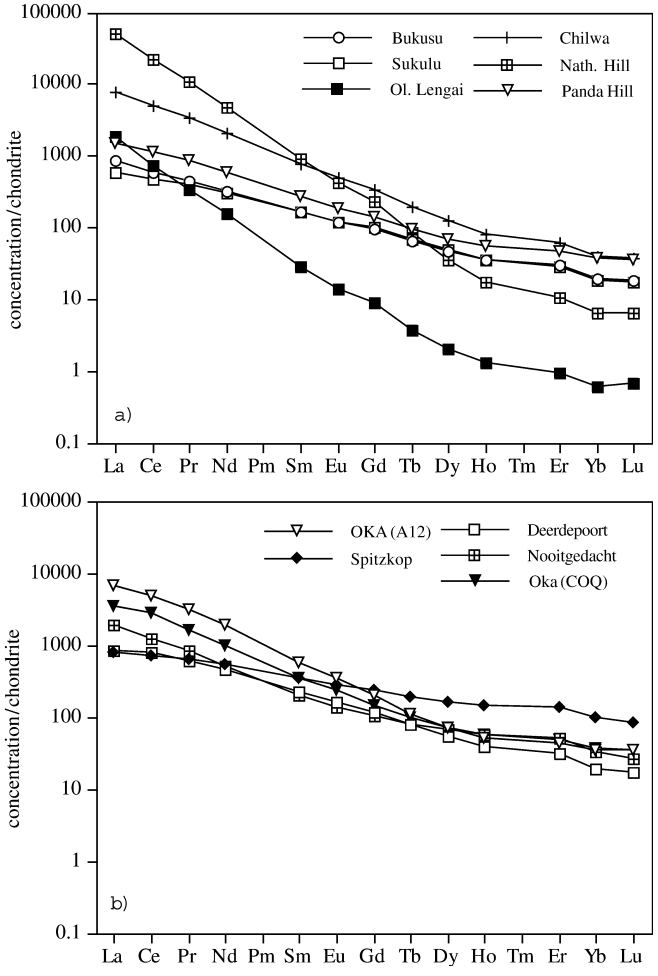

Fig. 1 Chondrite-normalized REE concentrations of carbonatites from this study. Chondrite values from Anders and Grevesse (1989). **a** East African rift samples, **b** samples from cratonic settings

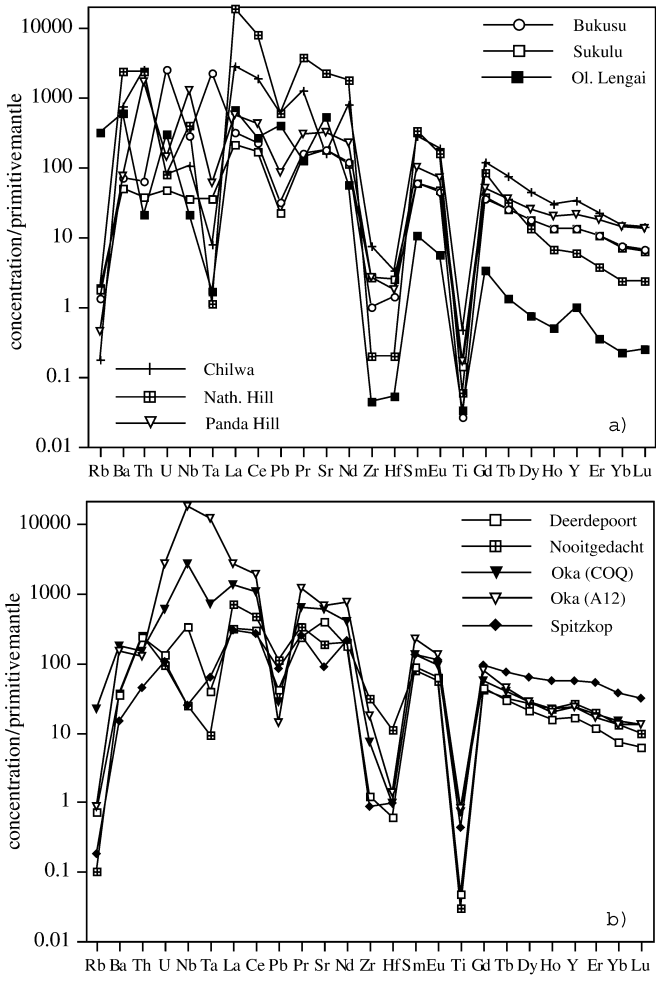

Fig. 2 Primitive mantle–normalized trace element concentrations of carbonatites. Normalization values from McDonough and Sun (1995). **a** East African rift samples, **b** samples from cratonic settings

limited variation in Nd and more variable Sr isotopes, while the carbonatites from Oka complex (Canada) have slightly more radiogenic Nd compositions (for a given Sr) than the East African carbonatites. The sample from Spitzkop complex plots close to the range reported by Harmer (1999) for this complex. The two Proterozoic samples from South Africa (Nooitgedacht and Deerdepoort) have similar Nd isotopic compositions as the Goudini carbonatite (Nelson et al. 1988) but show a large range in Sr isotopes (12ε_{Sr} units), forming a near horizontal array. We note that the ages of these Proterozoic complexes are not accurately known but they are believed to be between 1,400 and 1,200 Ma old (Harmer 1985; Nelson et al. 1988; Verwoerd 1967). Because of their low Sm/Nd and Rb/Sr ratios, the initial Nd and Sr isotopic compositions of these samples will not be significantly affected by the age uncertainty (± 3 ε units for ± 200 Ma uncertainty), therefore the larger variability in Sr isotopes for a given Nd appears to reflect that of their sources.

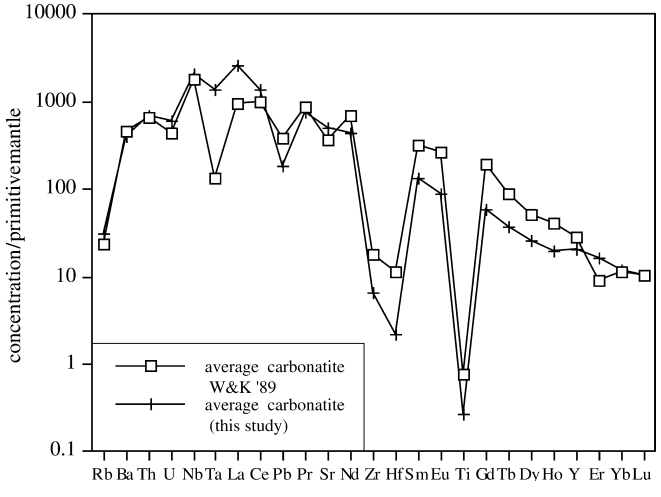

Fig. 3 Comparison between the average carbonatite from this study (Table 1) and the average calcio-carbonatite of Woolley and Kempe (1989). Normalization values from McDonough and Sun (1995)

Table 3 Measured and initial Sr, Nd and Pb whole rock isotopic compositions

Sample	$^{87}Sr/^{86}Sr$ Measured	$^{87}Sr/^{86}Sr$ Initial[a]	ε_{Sr} Initial	$^{143}Nd/^{144}Nd$ Measured	$^{143}Nd/^{144}Nd$ Initial	ε_{Nd} Initial	$^{206}Pb/^{204}Pb$ Measured	$^{207}Pb/^{204}Pb$ Measured	$^{208}Pb/^{204}Pb$ Measured	$^{206}Pb/^{204}Pb$ Initial	$^{207}Pb/^{204}Pb$ Initial	$^{208}Pb/^{204}Pb$ Initial
BD 724	0.703754	0.703754	−11.50	0.512561	0.512496	0.06	18.59	15.60	45.54	18.32	15.59	41.33
BD 114	0.704471	0.704471	−3.25	0.512615	0.512615	−0.45	19.20	15.58	39.21	19.20	15.58	39.21
BD 1476	0.703126	0.703126	−21.66	0.512818	0.512792	4.01	24.99	16.00	40.47	20.43	15.79	40.32
BD 1488	0.703184	0.703184	−20.84	0.512792	0.512764	3.47	21.11	15.79	40.40	20.99	15.79	40.28
BD 1584	0.703519	0.703519	−14.54	0.512712	0.512650	3.49	19.37	15.66	39.56	19.35	15.67	38.58
BD 1550	0.703103		−20.53	0.512686		4.08	20.12	15.74	41.63			
BD 1577	0.703663	0.703663	−12.50	0.512659	0.512627	3.05	18.97	15.60	39.56	18.95	15.60	38.65
A12	0.703270	0.703270	−18.42	0.512803	0.512760	5.14	47.82	16.97	40.60	8.33	15.07	38.24
COQ	0.703257	0.703252	−18.67	0.512777	0.512727	4.50	nd	nd	nd			
BD 1261	0.703241	0.703240	2.38	0.511635	0.510948	0.80	47.85	16.98	40.64	45.52	16.79	33.07
BD 1309	0.702862	0.702858	−3.05	0.511567	0.510474	−8.46	19.49	15.57	37.27	16.92	15.36	35.91
BD 1290	0.702432	0.702429	−10.39	0.511806	0.510999	0.00	24.78	16.15	54.94	17.24	15.53	38.63

[a]Initial values were calculated using the Rb/Sr, Sm/Nd, U/Pb and Th/Pb ratios determined by ICP-MS (Table 2) and the ages from Table 1. Initial ε_{Nd} and ε_{Sr} values were calculated using $^{143}Nd/^{144}Nd = 0.512638$and $^{147}Sm/^{144}Nd = 0.1967$ for chondritic earth and $^{87}Sr/^{86}Sr = 0.7047$and $^{87}Rb/^{86}Sr = 0.0847$ for Bulk Earth. The LaJolla Nd standard was measured at $^{143}Nd/^{144}Nd = 0.511846 \pm 0.000016$ (2 SD, $n = 31$) and the EA Sr standard at $^{87}Sr/^{86}Sr = 0.708006 \pm 0.000018$(2 SD, $n = 19$). Nd and Sr ratios were fractionation corrected using $^{146}Nd/^{144}Nd = 0.7219$ and $^{86}Sr/^{88}Sr = 0.1194$, respectively. In-run precision for all runs is better than the external reproducibility of the standards. Nd blank < 11 pg. ε values for sample BD 1550 are present day. Measured Pb isotope values are corrected for fractionation by 0.12%/amu, based on repeated measurements of the NBS 981 and the values reported by Todt et al. (1996). External reproducibility of the NBS 981 was 0.032%/amu ($n = 14$). nd = not determined

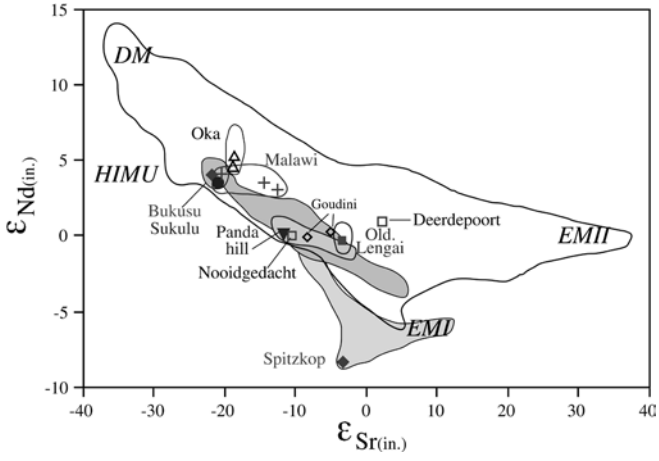

Fig. 4 Initial Nd and Sr isotope compositions of carbonatites from this study. Fields for each complex encompass this and published data. *Grey field* outlines data from other East African complexes not studied here. Data sources: Bell and Blenkinsop (1987, 1989); Bell and Tilton (2001); Dawson et al. (1995); Harmer (1999); Kalt et al. (1997); Nelson et al. (1988); Paslick et al. (1995); Simonetti and Bell (1994); Bell and Simonetti, (1996). Large field covers the global variation of MORBs and OIBs (data compilation from Stracke et al. 2003). Mantle end-member components (*DM*, *HIMU*, *EMI*, *EMII*) after Zindler and Hart (1986)

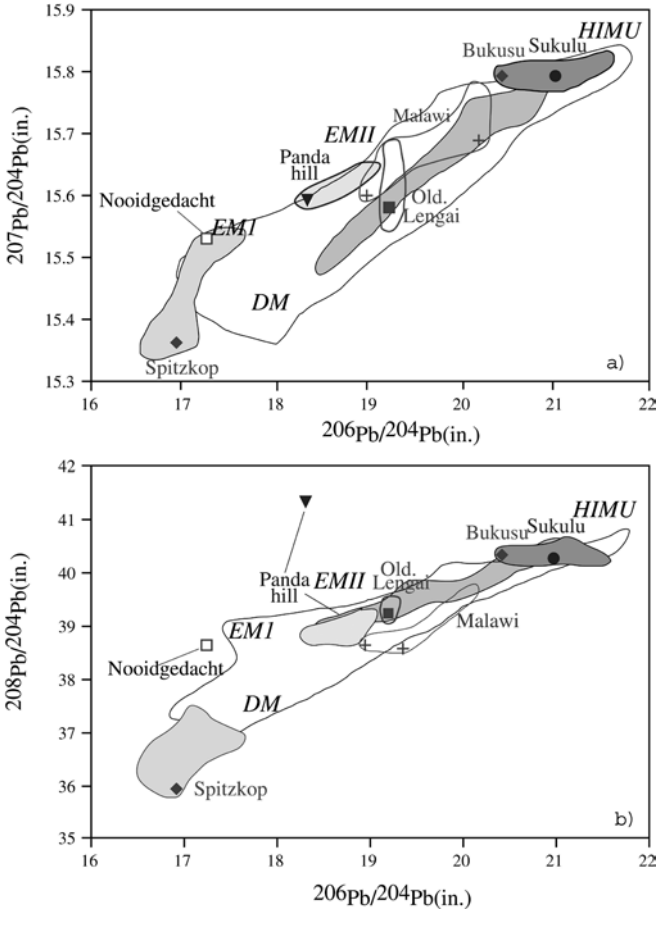

Fig. 5a, b Initial Pb isotope compositions of carbonatites from this study. Fields, symbols and data sources as in Fig. 4

Measured and initial Pb isotope compositions are presented in Table 3, and plotted in Fig. 5a, b. The data from the Bukusu and Sukulu samples fall close to previously determined data (Bell and Tilton 2001; Nelson et al. 1988) near the HIMU mantle end member. The sample from Oldoinyo Lengai falls within previous determinations, which form a vertical array on the $^{207}Pb/^{204}Pb$ vs. $^{206}Pb/^{204}Pb$ plot (Dawson et al. 1995; Bell and Simonetti, 1996). The data from the Panda Hill sample falls within the mantle array in the $^{207}Pb/^{204}Pb$ vs. $^{206}Pb/^{204}Pb$ plot, but above the array in the $^{208}Pb/^{204}Pb$ vs. $^{206}Pb/^{204}Pb$ diagram with relatively radiogenic $^{208}Pb/^{204}Pb$ ratio. On the $^{207}Pb/^{204}Pb$ vs. $^{206}Pb/^{204}Pb$ plot (Fig. 5a) the samples

from Malawi plot within the mantle array, extending towards the HIMU endmember. The data from the Spitzkop sample falls within the data of Harmer (1999) with relatively unradiogenic Pb isotope compositions.

Because of the large U/Pb and Th/Pb variations in these samples ($^{238}U/^{204}Pb = 1.15$ to 2315, $^{232}Th/^{204}Pb = 1.8$ to 751), some age corrections for the initial Pb isotopic compositions are large. For example, the calculated initial $^{206}Pb/^{204}Pb$ ratio for sample A-12 (Oka) is less than the value of the Canyon Diablo troilite (Table 3), which suggests some post-emplacement mobilization of U and/or Pb. For the samples with large age corrections on their Pb isotopic ratios, the initial Pb isotopic compositions are considered with caution.

Hf, Nd and Sr isotopic disequilibrium in carbonatites

Hf and trace element residence in carbonatites

In order to constrain the Hf, Zr and Ti residence in carbonatites we performed several dissolution experiments in which the carbonate fraction was preferentially dissolved (using HCl or HCl/HNO_3 mixtures) leaving an insoluble non-carbonate residue. The trace element concentrations of the carbonate and non-carbonate fractions were determined separately by solution ICP-MS (see Appendix) and the results are presented in Table 4 and plotted in Fig. 6. The data show that most of the Hf, Zr and Ti whole rock budget resides in the non-carbonate fraction (hereafter referred to as NC) while Sr and Nd budgets are dominated by the carbonate fraction (hereafter referred to as C). While the exact mineralogy of the NC fraction was not determined, the petrographic observations (Table 1) suggest that, in addition to silicate minerals, other non-silicate phases must be present in this insoluble residue (e.g. magnetite, pyrochlore, apatite, other oxides).

The C fractions have significantly higher Lu/Hf ratios than both the whole rock and the NC fractions, and usually contain less than 10% of the Hf whole rock budget. Similarly, Th, U, Nb, Ta along with Zr and Ti, are more enriched in the NC than the C fractions, while C dominates the REE and Sr whole rock budget. Certain ''spikes'' in the whole rock trace element patterns are controlled by the NC fraction, and are absent in the C fraction (e.g. U and Ta in the Bukusu sample, Nb in the COQ sample, Fig. 6). Where both NC and C fractions were measured, the whole rock concentrations can be reconstructed to better than 10%–15% for most elements (Table 4). In few cases (e.g. Nb and Ta in the Bukusu sample, Ti in the Chilwa sample, Nb in the Spitzkop sample) the reconstructed concentrations are considerably different from the measured whole rock. We attribute this to a "nugget" effect especially since Nb and Ta can be enriched in some trace mineral phases in carbonatites (e.g. pyrochlore). Nevertheless, most of the Hf, Zr, Ti, Nb, Ta, and sometimes Th and U whole rock budgets primarily reside in the non-carbonate fraction of carbonatites.

The most abundant non-carbonate minerals in carbonatites generally are apatite and magnetite (up to 5% by volume). Pyrochlore, zircon (baddeleyite or calzirtite), titanites, perovskite, magnetite, monazite, pyroxene, phlogopite, chlorite, and other Ba-Sr and REE-forming minerals are often also present in carbonatites but generally at lower abundances than apatite and magnetite (Dawson et al. 1996; Hogarth 1989; Hornig-Kjarsgaard 1998; Seifert et al. 2000). The large range in C/NC concentration ratios (up to three orders of magnitude for the LREE, Fig. 7) and the variability in these patterns is difficult to reconcile with the fractionation of a single (or a dominant) non-carbonate phase from a carbonatitic magma. Instead, this variation reflects the combination of different minerals in the NC fraction of carbonatites. However, common to all samples is that the whole rock Hf, Zr and Ti budgets primarily reside in the NC fraction, while Nd (REE) and Sr in the C fraction. This bimodal trace element distribution is significant in interpreting the Nd, Sr and Hf isotopic compositions of carbonatites: while the whole rock Nd and Sr isotope composition should reflect that of the carbonate fraction, the whole rock Hf isotope composition will be dominated by that of the non-carbonate fraction. Previous studies have suggested that some of the accessory minerals in carbonatites are xenocrysts (Barker 1996; Barker and Nixon 1989). This then requires us to investigate whether the non-carbonate and carbonate fractions are genetically related, in other words whether the two fractions are in isotopic equilibrium.

Hf, Nd and Sr isotope compositions in the carbonate and non-carbonate fractions

We determined the Nd, Sr and Hf isotopic compositions of the carbonate and non-carbonate fractions, using a modified Hf separation technique (see Appendix). Rb/Sr, Sm/Nd and Lu/Hf ratios in both fractions where determined by ICP-MS, while some of the Lu/Hf ratios in the C fractions were determined by isotope dilution. The Nd, Sr and Hf isotope data for the NC and C fractions are presented in Table 5. Using the trace element concentrations and isotopic compositions of the NC and C fractions, the Nd and Sr isotopic composition of the whole rock can be reconstructed to better than 1 ε unit for all samples. For the Hf isotopes, the agreement is better than 5 ε units (when taking the measurement errors into consideration), except for the Spitzkop sample. The overall isotopic and trace element agreement between reconstructed and measured whole rocks shows that we have not ''missed'' or ''over-sampled'' any of the NC or C fractions with the use of the separate dissolution technique.

Table 4 Trace element concentrations in the non-carbonate and carbonate fractions (ppm)

	BD 1476				BD 1488			BD 1584				COQ				BD1309				BD 1261	
Wt%	Carb 1[a] 99.6%	Silicate 0.4%	Diff%	Carb 2[b] 97%	Carb 1[a] 99.68%	Silicate 0.32%	Diff%	Carb 1[a] 97.1%	Silicate 2.9%	Diff%	Carb 2[b] 97.2%	Carb 1[c] 77%	Silicate 23%	Diff%	Carb 2[b] 92%	Carb[a] 99.8%	Silicate 0.2%	Diff%	Carb 2[β)] 98.9%	Carb 1[b] 83.0%	Silicate
Rb	0.73	2.17	−8	0.55	1.101	1.96	4	0.08	0.78	−2	0.07	16.18	1.72	−4	12.64	0.11	3.26	0	0.10	0.03	0.25
Sr	3452	299.2	−3	3832	3661	199.4	2	3245	5044	3	2997	13301	6264	−1	12664	1931	529.8	10	1777	4432	66.65
Zr	0.74	2661	1	1.54	0.47	9392	6	3.41	2260	−16	35.18	2.10	327.3	0	6.16	0.77	4226	−11	1.99	47.78	1649
Nb	2.35	4952	−792	15.27	1.62	6664	−2	2.05	2377	1	7.32	50	6330	−16	142	2.25	3282	−96	0.89	4.88	68.8
La	244.7	753.7	15	256	143.0	176	1	1876	837	3	1654	544	1841	−2	829.3	148.8	36655	12	123.1	234.9	1547
Ce	446.4	1161	18	480.7	304.7	1179	5	3251	896.4	3	2952	759.1	4860	−3	1248	376.9	66920	12	327.2	449.5	2458
Pr	49.6	104.9	19	53.31	37.42	30.70	5	326	57.66	3	297.3	78.19	376.2	−2	130.5	54.32	7108	12	47.76	51.74	213.5
Nd	176.5	300.9	17	190.6	142.9	108.8	1	1019	117.2	3	940.5	255	1143	−3	404.4	250.5	23068	11	218.2	179.9	557.6
Sm	28.93	20.78	16	30.98	24.95	13.2	1	123.0	12.28	2	113.1	25.34	144.9	−2	46.21	56.71	2026	12	51.14	27.7	50.15
Eu	8.10	3.67	15	8.80	7.02	3.33	1	29.96	4.75	4	27.71	6.42	38.48	−2	12.04	17.78	377.22	13	16.09	7.53	10.39
Gd	22.03	7.57	14	23.74	19.09	9.41	−4	68.50	18.52	1	63.19	15.06	76.39	−2	27.62	53.96	725.60	11	49.02	20.77	25.7
Tb	2.85	0.70	14	3.09	2.40	1.05	−4	7.30	6.05	−1	6.98	1.76	10.23	−3	3.36	8.12	52.19	12	7.32	2.90	3.61
Dy	13.94	2.95	15	14.83	11.71	5.07	−2	29.73	56.43	0	28.52	8.50	50.16	−2	16.30	46.18	171.51	11	42.10	15.02	25.95
Ho	2.39	0.48	15	2.55	1.98	0.91	−3	4.32	14.97	1	4.20	1.59	8.53	−2	2.95	9.43	23.78	12	8.66	2.62	6.66
Er	5.59	1.16	14	5.97	4.56	2.38	−4	8.54	50.80	0	8.66	3.94	21.61	−3	7.53	25.39	56.40	12	22.99	5.61	22.51
Yb	3.76	0.81	14	4.04	2.96	1.91	−4	5.19	57.63	0	5.52	2.55	18.51	−2	5.84	18.65	65.53	13	17.00	2.66	19.97
Lu	0.51	0.11	12	0.54	0.41	0.34	−6	0.71	8.56	0	0.77	0.367	2.46	−2	0.81	2.35	11.15	12	2.15	0.31	2.43
Hf	0.01	105.2	4	0.05	0.03	199.9	−3	0.03	28.06	−12	0.44	0.012	1.18	2	0.03	0.02	112.7	−2	0.04	0.40	15.73
Ta	0.04	2119	−922	0.54	nd			nd			0.11	3.90	94.12	−5	1.88	nd			0.10	0.02	1.92
Pb	5.32	11.29	9	4.90	3.68	16.02	10	96.88	23.14	4	83.13	4.65	2.98	3	3.93	13.36	55.01	13	9.14	17.37	11.79
Th	2.47	644.0	−2	2.45	1.49	429.1	−9	205.6	12.64	−3	184.1	2.45	45.89	7	7.76	3.58	367.8	16	3.17	6.20	82.36
U	4.69	12313	3	1.67	0.75	76.05	−29	1.41	9.01	2	0.94	4.70	32.61	−2	1.51	2.24	31.11	10	1.98	0.57	7.85
Ti	24.00	1274	−10	12.10	87.06	20410	−9	12.28	39075	51	51.77	404.3	2453	−2	250.3	64.28	225000	−9	7.06	11.39	157.5
Rb/Sr	0.0002	0.0072		0.00014	0.0003	0.0098		0.00002	0.00015		0.00002	0.0012	0.0003		0.001	0.00006	0.006		0.00006	0.00001	0.0037
Sm/Nd	0.164	0.069		0.163	0.175	0.121		0.121	0.105		0.120	0.099	0.127		0.114	0.226	0.088		0.234	0.154	0.090
Lu/Hf	51.3	0.001		11.4	15.8	0.002		23.7	0.305		1.7	30.3	2.083		23.3	95.1	0.099		48.6	0.778	0.155

Carb 1, 2, Silicate: carbonate and silicate fraction concentrations from different dissolutions.*Wt%*: is the percent weight of the carbonate and silicate phase relative to the whole rock.This was determined by weighing the dry silicate fraction after dissolution of the carbonate fraction, and comparing it with the whole rock weight. *Diff%* The percentage difference between the reconstructed and measured whole rock concentrations. nd = not determined

[a]Carbonate dissolution with HCL:HNO_3 (3:1)

[b]Carbonate dissolution with hot HCl

[c]Carbonate dissolution with cold 2.5 N HCl. Silicate fraction concentration for sample BD 1261 was estimate by mass balance between the carbonate and the whole rock

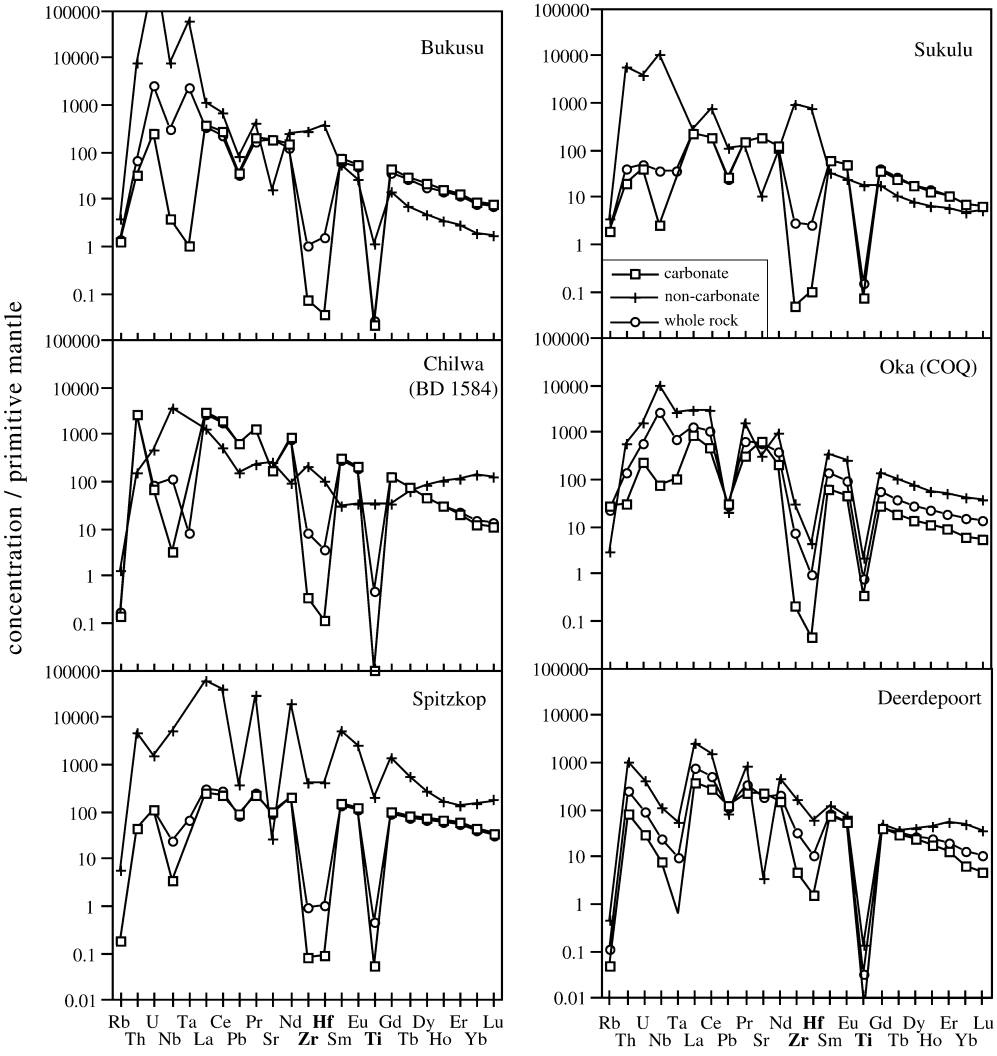

Fig. 6 Mantle-normalized concentrations for the non-carbonate and carbonate fractions, compared to the whole rock. y-axis scale is the same in all figures for comparison. Normalization values from McDonough and Sun (1995). Data from Table 4

The initial Nd and Sr isotopic compositions of the NC and C fractions are shown in Fig. 8. The C and NC fractions for the Oka samples (COQ, A-12) and Chilwa Island are in Nd and Sr isotopic equilibrium at the time of eruption, while all other samples show isotopic disequilibrium between the two fractions. The NC fractions of both Bukusu and Sukulu samples have less radiogenic initial $^{143}Nd/^{144}Nd$ ratios than the C. The NC fraction from the Panda Hill and Deerdepoort samples have more radiogenic Sr compositions (but similar Nd) than their C fractions, which are again identical to the whole rock. For the Spitzkop sample, the C is isotopically identical to the whole rock but the NC has more radiogenic Sr *and* Nd compositions. In general, while the Sr and Nd isotope compositions of the carbonate fractions are identical (within error) to the whole rock, the non-carbonate fractions are often in Nd and Sr isotopic disequilibrium with the carbonate.

Most of the measured $^{176}Hf/^{177}Hf$ ratios in the carbonate fractions are considerably more radiogenic than any oceanic island or mid ocean ridge basalt (Table 5). On a $\varepsilon_{Nd}/\varepsilon_{Hf}$ space (Fig. 9a, b) the initial Hf and Nd isotopic compositions of the NC fractions and the whole rocks fall close to or within the mantle array, consistent with the Nd and Sr isotope data (Fig. 8). However, the C fractions have much more variable initial ε_{Hf}, falling

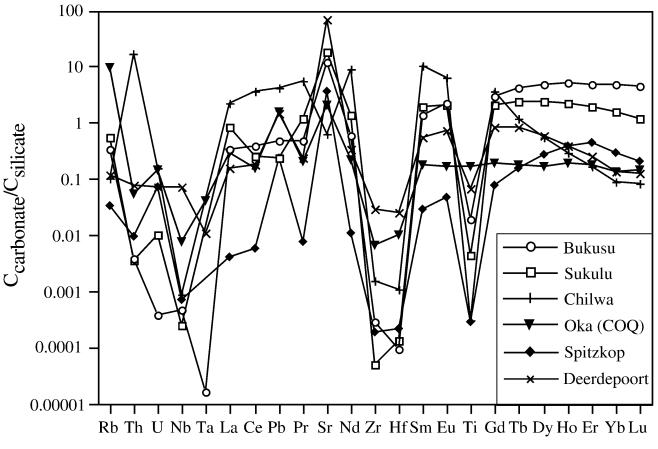

Fig. 7 Carbonate/non-carbonate concentration ratios

Table 5 Measured and initial Sr, Nd and Hfisotope compositions in the whole rock, silicate and carbonate fractions

Sample	$^{87}Sr/^{86}Sr$ Measured	Rb/Sr	$^{87}Sr/^{86}Sr$ Initial	ε_{Sr}	$^{143}Nd/^{144}Nd$ Measured	Sm/Nd	$^{143}Nd/^{144}Nd$ Initial	ε_{Nd}	$^{176}Hf/^{177}Hf$ Measured	Lu/Hf	$^{176}Hf/^{177}Hf$ Initial	ε_{Hf}
BD 1488 wr	0.703184	0.00030	0.703184	−20.8	0.512792	0.176	0.512764	3.5	0.283168 ± 53	0.628	0.283099	12.4 ± 2
NC[a]	0.703206	0.00980	0.703194	−20.7	0.512637	0.121	0.512618	0.6	0.282911 ± 15	0.0017	0.282911	5.8
NC[b]	0.703214		0.703214	−20.6					0.282895 ± 61		0.282895	5.2 ± 2
C[a]	0.703129	0.00030	0.703129	−21.6	0.512796	0.175	0.512768	3.6				
C[c]									0.283957 ± 262	20.0 $_{ID}$	0.281753	−34.7 ± 9
BD 1476 wr	0.703126	0.00023	0.703126	−21.7	0.512818	0.165	0.512792	4.0	0.282973 ± 33	1.121	0.282849	3.6
NC[a]	0.703229	0.00725	0.703217	−20.4	0.512710	0.069	0.512699	2.2	0.282742 ± 22	0.001	0.282742	−0.15
NC[b]	0.703243	0.00146	0.703241	−20.0								
C[a]	0.703167	0.00021	0.703167	−21.1	0.512820	0.164	0.512794	4.1				
C[b]	0.703099	0.00014	0.703099	−22.0	0.512826	0.163	0.512800	4.2				
C[c]									0.283761 ± 54	20.0 $_{ID}$	0.281554	−41.7 ± 2
COQ wr	0.703257	0.0011	0.703252	−18.7	0.512777	0.115	0.512727	4.5	0.284539 ± 35	3.141	0.283600	31.7 ± 2
NC[b]					0.512820	0.114	0.512770	5.3	0.283329 ± 85	0.284	0.283185	17.1 ± 4
C[b]					0.512770	0.114	0.512720	4.4	0.298242 ± 26	50.17	0.283219	19 ± 15
C[c]									0.297867 ± 128	49.35$_{ID}$	0.283010	14.3 ± 7
BD 1584 wr	0.703519	0.000032	0.703519	−14.5	0.512712	0.121	0.512650	3.5	0.283254 ± 77	0.989	0.282901	7.5 ± 4
wr duplicate									0.283241 ± 60	0.989	0.282888	7 ± 3
NC[a]	0.703564	0.000155	0.703563	−13.9	0.512708	0.105	0.512654	3.5	0.282848 ± 14	0.305	0.282739	1.7
NC[b]									0.282901 ± 29	0.377	0.282766	2.7
C[a]	0.703533	0.000025	0.703533	−14.3	0.512709	0.121	0.512647	3.4	0.289723 ± 450	23.78	0.281238	−51.3 ± 22
C[c]									0.289372 ± 211	20.98$_{ID}$	0.281888	−28.3 ± 11
BD 1309 wr	0.702862	0.000065	0.702858	−3.1	0.511567	0.2053	0.510474	−8.5	0.312496 ± 73	8.963	< earth	?
NC[a]	0.703965	0.0062	0.703623	7.8	0.511066	0.088	0.510599	−6.0	0.282714 ± 28	0.099	0.282346	15.8
NC[b]	0.703908	0.0011	0.703847	10.2	0.511074	0.09	0.510595	−6.1	0.285070 ± 20	0.0207	0.284702	99.3
C[a]	0.702923	0.000056	0.702920	−2.2	0.511708	0.226	0.510504	−7.9	0.355350 ± 45	95.1	< earth	?
C[b]	0.702872	0.000057	0.702869	−2.9	0.511726	0.234	0.510479	−8.4				
C[c]									0.380434 ± 336	56.04 $_{ID}$	< earth	?
A12 wr	0.703270	0.000040	0.703270	−18.4	0.512803	0.099	0.512760	5.1	0.284142 ± 113	2.310	0.283451	26.4 ± 4
NC[a]	0.703238	0.000074	0.703238	−18.9	0.512768	0.081	0.512733	4.6	0.283459 ± 17	0.030	0.283448	26.4 ± 2
NC[b]									0.283570 ± 12	0.103	0.283539	29.6 ± 2
C[a]	0.703336	0.000038	0.703336	−17.5	0.512808	0.103	0.512763	5.2		335.8		
C[b]										279.3$_{ID}$		
BD 1261 wr	0.703241	0.000017	0.703240	2.4	0.511635	0.129	0.510948	0.8	0.282431 ± 14	0.228	0.281600	−10.7
NC[b]	0.706660	0.004	0.706450	48.0	0.511311	0.090	0.510832	−1.5	0.282285 ± 14	0.155	0.281731	−6.0
C[b]	0.703225	0.000007	0.703225	3.2	0.511717	0.154	0.510897	−0.2				
C[c]									0.282537	0.1315$_{ID}$	0.282048	5.2
BD 724 wr	0.703754	0.000044	0.703754	−11.5	0.512561	0.146	0.512496	0.06	0.282959 ± 40	1.834	0.282390	−10.9 ± 2
NC[a]	0.704039	0.000067	0.704038	−7.4	0.512564	0.121	0.512510	0.34	0.282892 ± 14	0.012	0.282888	6.6
C[a]	0.703753	0.000045	0.703753	−11.5	0.512558	0.143	0.512494	0.03		139.2		

[a,b,c]Symbols for dissolution method as in Table 4. wr, Whole rock (Nd, Sr data from Table 3), C, Carbonate fraction; NC, non-carbonate fraction. In run precision for all Sr and Nd measurements is better than the reproducibility of the standards (see Table 3). All concentration ratios byICP-MS, except where noted by isotope dilution (ID). Some concentrations are from Table 4, while for others the Sm/Nd, Rb/Sr and Lu/Hf ratios where determined by ICP-MS on a small aliquot of the dissolution. Where no data are reported, it was not determined. Initial $\varepsilon_{Sr}$and ε_{Nd} are calculated as in Table 3. Initial ε_{Hf}values calculated using present-day chondritic earth values of $^{176}Hf/^{177}Hf = 0.282772$,$^{176}Lu/^{177}Hf = 0.0332$,$\lambda = 1.9310^{-11}$ and the ages from Table 1. ε_{Hf} uncertainty is calculated assuming5% error on the Lu/Hf ratios (for the ICPMS measurements), and the uncertainty of the measurement. Where no errors are reported, these are less than 2 ε_{Hf}units. See Appendix for further details on Hf and Lu/Hf determinations

well below or close to the mantle array. The extreme Lu/Hf ratios in the carbonate fractions (Table 5) makes the calculation of their initial Hf isotopic composition very sensitive to the precise age of these rocks, while age effect on Nd and Sr isotopes is negligible because of the low Sm/Nd and Rb/Sr ratios for both C and NC fractions. Nelson et al (1988) reports an age range of 25–55 Ma for the Bukusu and Sukulu complexes (average 40 Ma; Table 1). For an age of 25 Ma, the initial ε_{Hf} of the C fraction for the Sukulu sample becomes $\varepsilon_{Hf} = -6$, and for Bukusu $\varepsilon_{Hf} = -12.9$, i.e. 28.8 ε_{Hf} units higher than the initial ε_{Hf} values if the 40 Ma age is used (Table 5). In either case (for both ages), both samples have strong Hf isotopic disequilibrium between their C and NC fractions. Similarly, for the Chilwa sample, the initial Hf isotopic composition of the C fraction is highly unradiogenic (Fig. 9a, $\varepsilon_{Hf} = -40$, average of the two measurements from Table 5). The reported ages for the Chilwa Island complex are 138 ± 7 and 126 ± 8 Ma (Simonetti and Bell 1994) and 135–105 Ma for the Chilwa alkaline province (Woolley and Jones 1987). For an age of 118 Ma (the youngest age estimate for Chilwa complex), the initial ε_{Hf} for the carbonate phase becomes $\varepsilon_{Hf} = -14$, i.e. 26 ε_{Hf} units higher than the calculated value for the 130 Ma age, again showing the sensitivity of the calculated initial ε_{Hf} on the precise knowledge of the eruption age. As for the Ugandan samples, the Chilwa sample also shows significant Hf isotopic disequilibrium between NC and C fractions. For sample COQ (Oka complex), both C and NC fractions have nearly identical initial ε_{Hf} (Fig. 9b) and a four-point Hf "isochron" gives an age of 106 ± 3 Ma, within error to

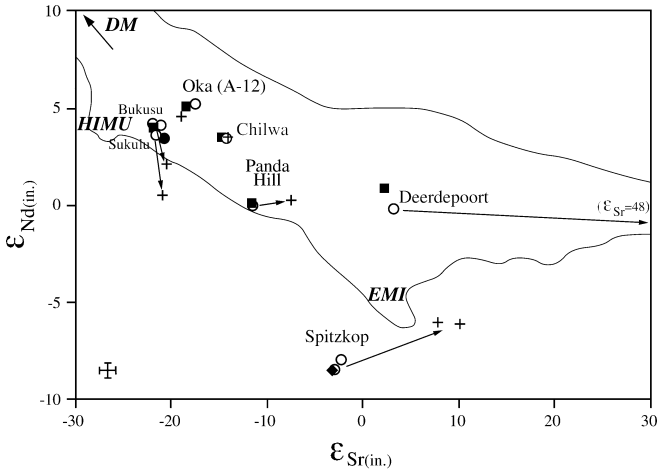

Fig. 8 Initial Nd and Sr isotopic compositions of the whole rock, carbonate and non-carbonate fractions in carbonatites. *Circles* Carbonate fractions; *crosses* non-carbonate fractions; *filled squares* whole rock. Data from Table 5. *Arrows* point from the carbonate to the non-carbonate fraction of each sample. Outline of the mantle array and location of the mantle end-member components as in Fig. 4

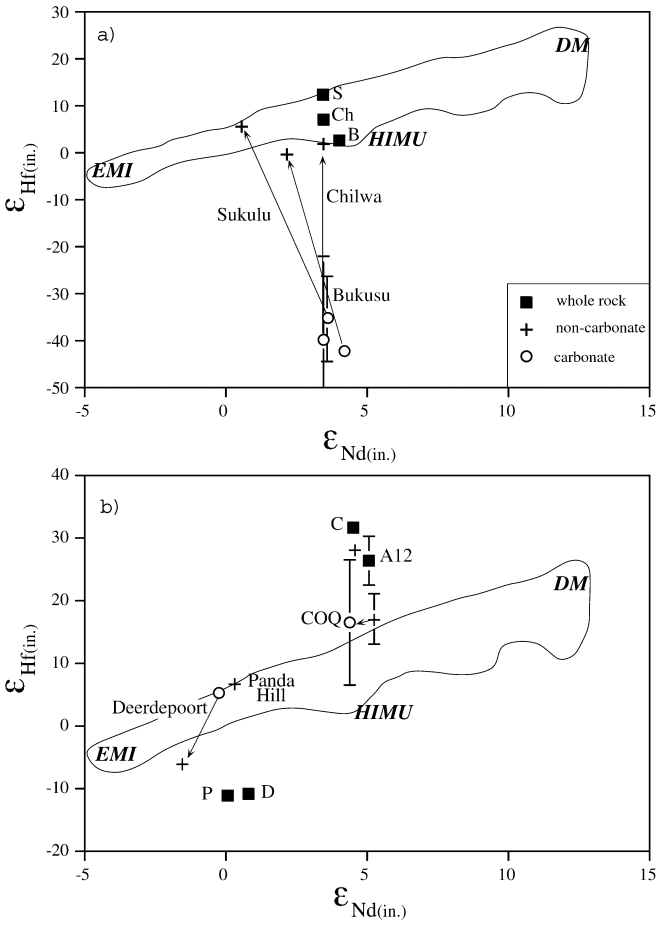

Fig. 9a, b Initial Nd and Hf isotopic compositions of whole rock, carbonate and non-carbonate fractions in carbonatites. *Circles* Carbonate fractions; *crosses* non-carbonate fractions; *squares* whole rock. Data from Table 5. Where more than one determination in Nd and /or Hf isotopes is available, the average is plotted. Error bars are the measurement errors (Table 5). *Arrows* point from the carbonate to the silicate fraction of each sample. *Letters next to squares* mark the whole rock compositions: *B* Bukusu, *S* Sukulu, *Ch* Chilwa, *D* Deerdepoort, *P* Panda hill, *C* COQ (Oka). Two panels are shown for clarity. *Outline* encompasses the total variation of MORB and OIB. Data from Spitzkop is not shown because the initial $^{176}Hf/^{177}Hf$ of the whole rock and carbonate fractions are lower than the initial $^{176}Hf/^{177}Hf$ of the earth

the 109 ± 2 Ma age given by Wen et al. (1987). With a Lu/Hf ratio of 50.1 in the C fraction (Table 5), only a 5 Ma age uncertainty results in a 25 ε_{Hf} unit uncertainty in the calculated initial ε_{Hf} composition. The NC fraction and whole rock for the other Oka sample (A-12) also appear in Hf and Nd isotopic equilibrium, mainly because C is practically devoid of Hf (Table 5).

The initial ε_{Hf} of the C fraction for the Deerdeport sample falls within the OIB array but the C, NC fractions and whole rock are in Hf isotopic disequilibrium (Fig. 9b). For the Panda Hill sample, the NC fraction and whole rock are in Hf isotopic disequilibrium, as also seen in the Sr isotopes. For the Spitzkop sample, the calculated initial $^{176}Hf/^{177}Hf$ is lower than the initial $^{176}Hf/^{177}Hf$ ratio of Bulk Earth for both whole rock and carbonate fractions. The Hf isotopic composition of the samples BD 1290, BD 114, and BD 1577 were not determined because of their very low Hf contents (Table 2).

In summary, the combined Nd, Sr and Hf isotopic compositions and trace element contents in the whole rock, carbonate and non-carbonate fractions of these carbonatite samples show frequent Nd and/or Sr and/or Hf isotopic disequilibrium between the different fractions. This isotopic disequilibrium strongly suggests that either (1) the non-carbonate fractions are exclusively xenocrysts in these carbonatites and not genetically related to the carbonate fraction or (2) *most* of the Hf, Nd and Sr elemental budget in the non-carbonate is xenocrystic in origin. In other words, even if some of the mineral phases in the NC fraction precipitated or are in isotopic equilibrium with C, the majority of the Hf and/or Nd and/or Sr budget in NC fraction must reside in some xenocrystic material. This conclusion is also supported by the highly variable trace element concentrations between C and NC fractions (Fig. 7). Since the carbonate fraction dominates the volume of the whole rock (>90%) as well as the elemental budget for most elements, it is suggested here that the trace element and isotopic composition of the carbonate fraction is more representative of the carbonatitic magma as this rises from the mantle, than the whole rock carbonatite. As such, the isotopic and trace element composition of the *carbonate fraction* should *more closely* reflect the isotopic and trace element composition of the carbonatite source. We use this observation and our new trace and isotope data to constrain the origin of carbonatites and the evolution of their sources.

Discussion: the source of carbonatites

The origin of carbonatites has been extensively debated in the literature (see Bailey 1993; Bell et al. 1998; Wyllie and Lee 1998, for recent reviews). There are three general models suggested for the origin of carbonatites: primary magmas from the mantle, products of extensive crystal fractionation from a carbonated silicate magma, and immiscible liquids from a CO_2–rich silicate magma. All three models are supported by both experimental and field observations.

Carbonatites as primary mantle melts

There is ample experimental evidence suggesting that carbonatitic magmas exist in equilibrium with a mantle peridotite at pressures generally above 2.2 GPa (e.g. Dalton and Wood 1993; Lee et al. 2000; Moore and Wood 1998; Wallace and Green 1988; Wyllie and Huang 1975) and up to 7.0 GPa (Dalton and Presnall 1998). These melts are more Mg-rich than the Ca-rich carbonatites most frequently observed on the surface (Woolley and Kempe 1989). Calcio-carbonatite melts, however, are in equilibrium with wehrlite at pressures down to 1.5 GPa (Dalton and Wood 1993). These results were used to suggest that primary, mantle-derived Mg-rich carbonatite melts, upon ascent through the lithosphere, will react and convert lherzolite to wehrlite with concomitant shift of the melt compositions to that of Ca-rich carbonatite (Green and Wallace 1988; Dalton and Wood 1993; Harmer and Gittins 1998). Upon establishing opx-free conduits (i.e. wehrlite), subsequent primary carbonatitic melts could erupt directly to the surface.

Experimental partitioning data between carbonatite melts and peridotite minerals suggests that Hf, Zr and Ti will fractionate from the adjacent REE resulting in Hf, Zr and Ti depletions in the carbonatitic melt (Adam and Green 2001; Blundy and Dalton 2000; Green et al. 1992; Sweeney et al. 1995). Table 6 shows the estimates for bulk peridotite/carbonatite partition coefficients (lherzolite with or without garnet and/or amphibole), based on published mineral/ carbonatite partitioning data. Because of the scarcity of Hf and Lu partition coefficients, we also use Zr as a proxy for Hf and Yb for Lu. These data show that Hf (Zr) is nearly *equally* or *less compatible* than Lu (Yb) in a peridotite in equilibrium with a carbonatite melt (Table 6). Although Hf (Zr) is, on average, slightly more compatible than Lu (Yb) in clinopyroxene and amphibole, this leverage is reduced by the higher D_{Lu}/D_{Hf} in orthopyroxene and olivine (Salters and Longhi 1999; Salters et al. 2002, Blundy and Dalton 2000). If garnet is also present in the source, then Lu (Yb) becomes significantly more compatible than Hf (Zr) (Table 6). This relative compatibility of Lu and Hf in the peridotite then suggests that if carbonatites are primary melts (at least the Mg-rich ones), then the Lu/Hf ratio of the carbonatite source will be *nearly equal* or *higher* than the measured Lu/Hf in the carbonatite melt. In the case of the calcio-carbonatites as derivatives from the Mg-rich variety (Dalton and Wood 1993; Harmer and Gittins 1998), this conclusion is still valid, because dissolution of enstatite and precipitation of cpx (and olivine, see Eq. 3 of Moore and Wood 1998) *cannot significantly fractionate* Lu from Hf (Table 6).

Table 6 Average partition coefficients forclinopyroxene, garnet, amphibole in equilibrium with a carbonatite melt, and calculated bulk partition coefficients for a carbonatite source

Mineral	cpx	gar	amph	Bulk D gar. lherz	Bulk D sp. lherz	Bulk D amph. lherz
D_{Nd}	0.18	0.023	0.05	0.027	0.035	0.028
D_{Sm}	0.18	0.075	0.1	0.032	0.036	0.033
$D_{(Zr,Hf)}$	0.46	1.29	0.48	0.134	0.092	0.102
D_{Ti}	0.73	0.99	2.61	0.277	0.180	0.342
$D_{(Lu,Yb)}$	0.44	9.46	0.16	0.476	0.120	0.104
$D_{(Lu,Yb)}/D_{(Hf,Zr)}$	0.96	7.36	0.33	3.54	1.30	1.02
D_{Sm}/D_{Nd}	1.00	3.26	2.00	1.20	1.04	1.19
$D_{(Zr,Hf)}/D_{Sm}$	2.56	17.13	4.83	4.22	2.55	3.11
D_{Ti}/D_{Sm}	4.06	13.20	26.10	8.71	5.01	10.42

Cpx, clinopyroxene; gar, garnet;, amph, amphibole. Cpx, gar, and amph partition coefficients are averages from published mineral/ carbonated coefficients. Data sources: Blundy and Dalton (2000), Klemme et al. (1995), Green et al. (1992), Sweeney et al. (1992), Sweeney et al. (1995), Adam and Green (2001).$D_{(Zr,Hf)}$, $D_{(Lu,Yb)}$ are the average D_{Zr}, D_{Hf} and D_{Lu}, D_{Yb} taken from these studies. Bulk partition coefficients for different peridotite mineral assemblages are calculated using D^{cpx}, D^{gar}, D^{amph} from this table and D^{opx}, from Salters et al. (2002; experiment. RD 1097-2) and $D^{olivine}$ from Blundy and Dalton (2000). $D_{Nd}{}^{garnet}$ estimated by the average $D_{Sm}{}^{garnet}/D_{Nd}{}^{garnet} = 3.2$ (Salters et al. 2002) and $D_{Nd}{}^{amph}$ is assumed half of $D_{Sm}{}^{amph}$. Mineral modes: Garnet lherzolite: ol = 0.60, opx = 0.20, cpx = 0.12, gar = 0.04, amph = 0.04, Spinel lherzolite: ol = 0.60, opx = 0.22,cpx = 0.18, gar = 0, amph = 0, Amphibole-spinel lherzolite: ol = 0.60, opx = 0.2, cpx = 0.12, gar = 0, amph = 0.08

Using the measured Hf isotopic compositions and the Lu/Hf ratios of the carbonate fractions (Table 5), along with the arguments on the Lu/Hf partitioning between the carbonatitic melt and its source, we can put constraints on the age and isotopic evolution of the carbonatite source. Figure 10 shows the Hf isotopic evolution of the *carbonate fractions* determined here. We used the carbonate fractions only since, as suggested above, they more closely represent the composition of a carbonatitic melt. Based on the partitioning arguments, the slopes of these evolution curves represent the *minimum* slope of the evolution of their sources, since the Lu/Hf ratio of the source should be nearly *equal or greater* than that of the carbonatite (i.e. the higher the Lu/Hf ratio the steeper the slope). It can be seen from Fig. 10 that, if any of these carbonatite sources originated from any known terrestrial reservoir (between MORB and crust evolution curves), within only 10–25 Ma they would generate compositions that fall outside the compositions of any known terrestrial magma. Furthermore, if the time difference between source formation and eruption is greater than 30–50 Ma

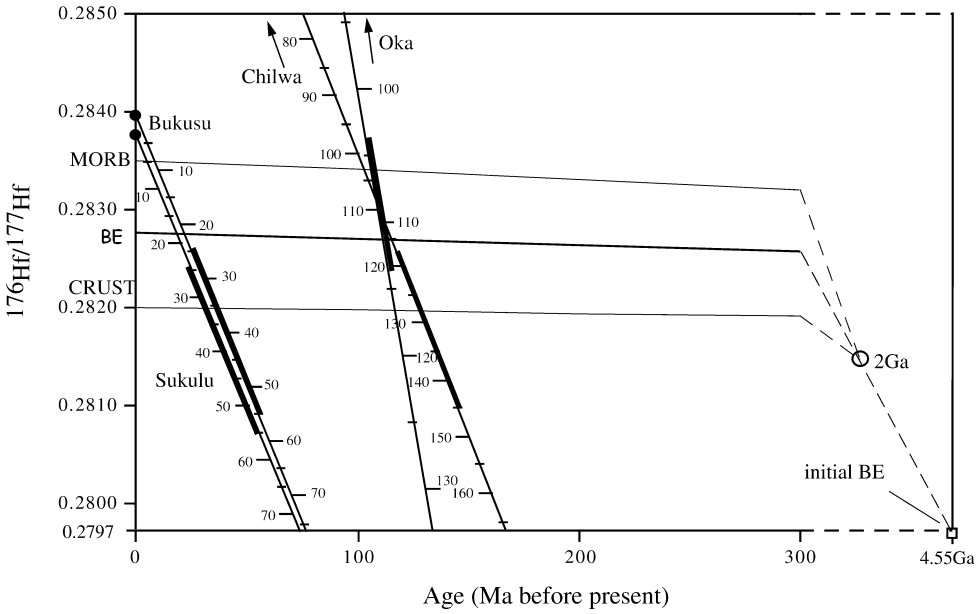

Fig. 10 Hf isotopic evolution of the carbonate fractions. We assume that MORB and CRUST reservoirs are formed 2 Ga ago from chondritic earth, and evolve to present-day values of 0.2835 and 0.2820, respectively. If an older age of formation is assumed (e.g. 3 Ga), it will not significantly affect the modeling and conclusions. Note the scale break after 300 Ma on the horizontal axis. Each sample evolution curve begins at present day with the measured $^{176}Hf/^{177}Hf$ ratio and evolve back in time based on the measured Lu/Hf ratios (Table 5). *Tick marks* on the evolution curves are at 5-Ma intervals and *numbers along tick marks* are in Ma before present. Present-day $^{176}Hf/^{177}Hf$ ratios for the Chilwa (average of the two determinations in Table 5) and Oka samples are not shown for clarity. Thicker segments along each evolution curve show the uncertainty on the initial Hf composition for each sample based on the uncertainty of the age of eruption: *Bukusu* and *Sukulu* 25–40 Ma, *Chilwa* 118–136 Ma, *Oka* 104–114 Ma. Since the Lu/Hf ratio in the carbonatite source is expected to be greater or equal to the Lu/Hf ratio of the carbonatite (see text), these slopes represent the minimum slopes of the evolution of these carbonatite sources

(irrespective of the uncertainties on the eruption ages), the initial Hf isotopic composition of all these carbonatite sources would have to be lower than the initial $^{176}Hf/^{177}Hf$ ratio of Bulk Earth. Therefore, the sources of these carbonatites could not have existed in the mantle (or even crust) for any period longer than 10–50 Ma.

The short residence time of these carbonatite sources is also shown in a conventional Nd/Hf isotope correlation diagram (Fig. 11), using the same arguments for the fractionation of Sm/Nd as for the Lu/Hf fractionation between a carbonatitic melt and its source. Nd is more incompatible than Sm in a peridotitic mineralogy in equilibrium with a carbonatite melt (Table 6) therefore, the carbonatite source will have higher Sm/Nd than the carbonatite melt. Fig. 11 shows the combined Nd and Hf isotopic evolution of the carbonate fractions. The slopes of the evolution curves again represent the minimum slope of the evolution of the carbonatite sources. Such carbonatite sources will evolve essentially vertical relative to the terrestrial array and will transverse the width of the array within only 10–15 Ma upon formation. For Sm/Nd ratios higher than chondritic earth (Sm/Nd >0.325, as for a depleted reservoir) the evolution lines change to positive slope but they remain very steep relative to the terrestrial array even for Sm/Nd ratios such as expected for the MORB source (Sm/Nd $=0.4$; Salters and Stracke, submitted).

Similar results are obtained for a model carbonatite-metasomatized mantle source. Fig. 11 shows the *present day* isotopic composition of a metasomatized source generated 100 Ma to 1 Ga ago by the addition of 1%–5% carbonatite melt to a peridotite with a primitive mantle composition. Such a metasomatized source will evolve over time towards radiogenic Hf and unradiogenic Nd compositions, almost at a right angle to the terrestrial array. The width of the terrestrial array allows for a maximum of 200–300 Ma isolation of a carbonatite-metasomatized source before it develops compositions that fall outside those of any terrestrial magmas (Fig. 11). If any other source within the array is used for the calculations it too will evolve near parallel to the curves shown here, since the metasomatizing carbonatite dominates the Sm and Nd concentrations and the relative fractionation of Lu/Hf vs. Sm/Nd.

The robust slope of the terrestrial array in the Nd/Hf space suggests that the time- integrated (Lu/Hf)/(Sm/Nd) fractionation in the earth system has remained relatively constant throughout most of earth's history (Salters and White 1998; Vervoort et al. 1999). A carbonatite source generated within the array will evolve over short time (ca. 15 Ma) well outside the compositions of terrestrial magmas, while a carbonatite-metasomatized source can exist for up to 300 Ma before it generates Nd and Hf compositions outside the array (Figs. 10, 11). The absence of any such radiogenic Hf isotopic compositions in the terrestrial magmas (including the carbonatites measured here) then suggests that carbonatite sources must have a *very short residence*

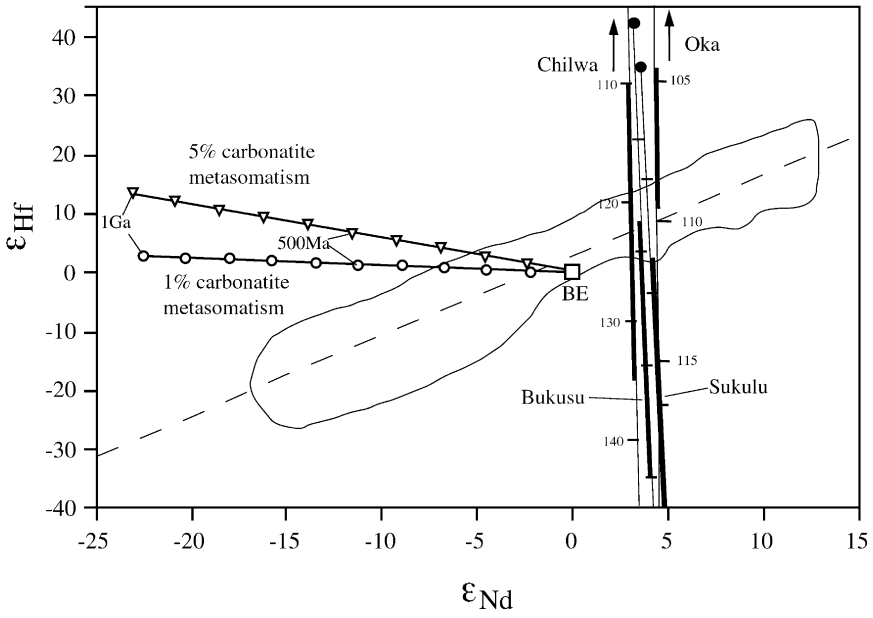

Fig. 11 Nd vs. Hf isotopic evolution of the carbonate fractions and of a carbonatite-metasomatized source. *Outlined field* includes both oceanic and crustal samples and *dashed line* is the regression line of the terrestrial array after Vervoort et al. (1999). The evolution curves for the carbonate fractions are calculated using the measured Nd and Hf isotope ratios and the Sm/Nd and Lu/Hf ratios from Table 5. The plotted ε_{Nd} and ε_{Hf} compositions are initial values at time T in the past. *Tick marks* along the evolution lines are at 10-Ma intervals starting from present day. Age (in Ma) along tick marks is shown for the Chilwa and Oka samples. Thicker segments along the evolution curves as in Fig. 10. Present-day compositions for the Chilwa and Oka samples are not shown for clarity. Based on the partition coefficients between a carbonatite and a peridotite (see text), the slopes of these curves represent the minimum slope of the evolution of the carbonatite sources. *Lines with circles and triangles* represent the *present day* Nd and Hf isotopic composition of a mantle source that was metasomatized by 1% to 5% carbonatitic melts 100 Ma to 1 Ga ago. Both mantle source and metasomatizing carbonatite are assumed to have Bulk Earth isotopic composition at the time of metasomatism. Bulk Earth Nd, Sm, Lu and Hf concentrations from McDonough and Sun (1995). Carbonatite Nd, Sm and Lu concentrations from Table 2 (average values). Hf concentration is calculated by using Lu/Hf = 20 from Table 5, the minimum Lu/Hf fractionation measured in the carbonate fractions

time in the mantle. Alternatively, if long-lived carbonatite sources *do* exist in the mantle, then they must be a volumetrically insignificant component of the mantle and they do not appreciably contribute to any other types of known volcanism.

As noted by Adam and Green (2001) and Blundy and Dalton (2000), the extreme LREE enrichments and the Hf, Zr and Ti decoupling from the REE in carbonatites cannot be reconciled with the current peridotite-mineral/carbonatite experimentally determined partition coefficients. Furthermore, the Lu/Hf ratios in these carbonatites (the carbonate fractions) range from 20–279 (Table 5, except sample BD 1261), which are 83–1,160 times greater than the primitive mantle Lu/Hf ratio of 0.238 (McDonough and Sun 1995). The maximum Lu/Hf fractionation between a source and melt that can be achieved during melting is determined by D_{Lu}/D_{Hf}, which is close to or greater than unity (Table 6). This suggests that a carbonatite source must have significantly different Lu and Hf concentrations than primitive or depleted mantle. Therefore, previous metasomatic event(s) are necessary to generate such a source, which must involve the addition of a CO_2-rich melt/fluid, fractionation of Hf and Zr from the REE and enrichment in LREE, Ba, Sr and other incompatible elements. Irrespective of these processes, if carbonatites are near primary mantle melts, then their source must be a short-lived one.

Carbonatites as crystal fractionates or immiscible liquids

The almost universal association of carbonatites with alkali silicates rocks in the field has led to the proposal that carbonatites are products of immiscibility from an alkali silicate melt or the residues of extreme crystallization. There is abundant experimental data on carbonate-silicate liquid immiscibility, both in model and natural compositions as well as petrographic and field evidence supporting the two hypotheses (Brooker 1998; Church and Jones 1995; Dawson et al. 1994; Kjarsgaard 1998; Lee and Wyllie 1997b; Petibon et al. 1998; Schleicher et al. 1990, and references therein). However, the frequent isotopic disequilibrium between carbonatites and associated silicate rocks (Bell 1998; Harmer and Gittins 1998) and the almost universal later emplacement of carbonatites relative to the silicate rocks (Barker 1989; Harmer and Gittins 1997), casts doubts on the association of the two rock types by fractionation or immiscibility.

It is well beyond the scope of this paper to examine the details of immiscibility and crystal fractionation for the genesis of carbonatites, and quoting Bell et al (1998) "...Clearly, there are carbonatites and carbonatites".

However, we examine our data under the scope that some carbonatites are indeed the products of immiscibility and/or crystal fractionation.

As shown earlier (in the sectionHf, Nd and Sr isotope compositions in the carbonate and non-carbonate fractions; Figs. 7, 8, 9) the isotopic dissequilibrium between the NC and C fractions, is inconsistent with the two fractions being genetically related. Therefore, the NC fraction cannot be a product of immiscible or fractionated (silicate or otherwise) phases from the C fraction which, we suggest, better represents the composition of a carbonatitic magma. From an "isotopic" point of view then, we do not see evidence for fractionation or liquid immiscibility within the analyzed samples.

It is possible, however, that crystallization or immiscibility could have taken place in a deeper magma chamber (Petibon et al. 1998), in which case the trace element fractionation in carbonatites cannot be directly related to their source. Considering that the experimentally produced silicate-carbonate phase associations are complicated at best (e.g. Lee and Wyllie 1997a, 1997b), we nevertheless try to estimate the trace element fractionation during crystallization or immiscibility. The experiments on the nephelinite-dolomite-$NaCO_3$ joint (Lee and Wyllie 1997a) crystallized olivine, clinopyroxene plus traces of spinel along with quenched silicate and carbonate liquids and calcite. As it was shown earlier (see Table 6, and Carbonatites as primary mantle melts), these minerals cannot significantly fractionate Lu from Hf. In the Mg-free system Na–Al–Ca–Si + CO_2, Lee and Wyllie (1997b) report melilite, anorthite, nepheline, scapolite along with immiscible silicate and carbonatite liquids. The few available partition coefficients for melilite and nepheline (Kuehner et al. 1989; Larsen 1979), also suggest no significant fractionation between Zr and Yb (and by inference Lu and Hf).

Kjarsgaard (1998) reports melanite (garnet), perovskite, wollastonite, titanite, apatite in immiscibility experiments. Of these, perovskite and titanite (using rutile as a proxy) have $D_{Hf} > D_{Lu}$, (Foley et al. 2000; Kato et al. 1988), while melanite (garnet) should have $D_{Lu} > D_{Hf}$ (Sweeney et al. 1992). If such phases precipitate from carbonatite melts, and are responsible for the observed HFSE/REE fractionation at mid-crustal levels, then crystallization of titanite/perovskite must dominate over melanite, since these minerals will fractionate Lu/Hf the opposite way. Finally, the immiscibility partitioning experiments of Veksler et al. (1998) and Hamilton et al. (1989) show preferential partitioning of Zr and Hf over the REE in the immiscible silicate liquid. However, these partition coefficients cannot generate the extreme LREE/HREE ratios of carbonatites without the progenitor carbonated-alkali-silicate melt being already highly enriched in these elements.

If either or both silicate immiscibility and titanite/perovskite (even zircon) fractionation are responsible for the ubiquitous HFSE/REE decoupling in carbonatites, then these processes must be very robust and reproducible in the lithosphere, leaving a high HFSE/REE residue. In this case, the (now evolved) carbonatitic melt that erupts on the surface must be near perfectly separated from the fractionated silicates, while becoming contaminated by other phases en route to the surface, in order to generate the observed isotopic dissequilibrium.

We conclude that the trace element and isotopic compositions of carbonatites must closely represent that of their source, unless some highly specific and reproducible fractionation and/or immiscibility process(es) takes place within the lithosphere. As such, the Lu/Hf isotope systematics of carbonatites suggest that their sources must be short lived features in the mantle and probably melt out soon after formation. On the other hand, if the trace element fractionation in carbonatites does not represent that of their sources, then the *lack of* radiogenic Hf compositions in carbonatites again suggest that their source does not have long lived Hf (Zr and Ti) depletions.

Origin of the East African carbonatites

The combined Nd, Sr and Pb isotopic compositions of carbonatites and other alkali basalts associated with the East African Rift suggest mixing between a HIMU and EMI-type mantle components (e.g. Paslick et al. 1995; Bell and Simonetti 1996; Bell and Tilton 2001; Figs. 4, 12). This HIMU-EMI type mixing though is rarely observed in OIBs. Only samples from the Austral-Cook Island chain show such a mixing trend, while the isotopic compositions of most of the other ocean islands suggest mixing between either EMI, EMII and HIMU components and a component internal to the OIB field, PREMA (Zindler and Hart 1986), FOZO (Hart et al. 1992) or C (Hanan and Graham 1996; Fig. 12). Furthermore, the HIMU-type East African carbonatites generally have higher $^{87}Sr/^{86}Sr$ than the HIMU-type OIBs (Fig. 12). Kalt et al. (1997) suggested that such isotope characteristics originate from a heterogeneous lithospheric mantle that was produced by various enrichment and depletion events at different times in the past. Paslick et al. (1995) also suggested that the northern Tanzanian volcanics originate from a subcontinental lithospheric mantle source which acquired its trace element enrichment and isotopic composition through underplating of OIB-type melts ca. 2 Ga ago. Alternatively, Bell and Simonetti (1996) suggested that the East African volcanics result from a recently metasomatized EMI-type lithosphere by an upwelling mantle cell or plume of HIMU affinities. Recently, Bell and Tilton (2001) suggested that the EMI–HIMU mixing reflects the heterogeneous nature of a mantle plume that carries both these components from deep in the mantle.

As suggested earlier, the Lu/Hf isotope systematics of carbonatites requires that the carbonatite source must be a short-lived feature in the mantle. In this case, an ancient, metasomatized lithospheric source for these carbonatites (Kalt et al. 1997; Paslick et al. 1995) is not

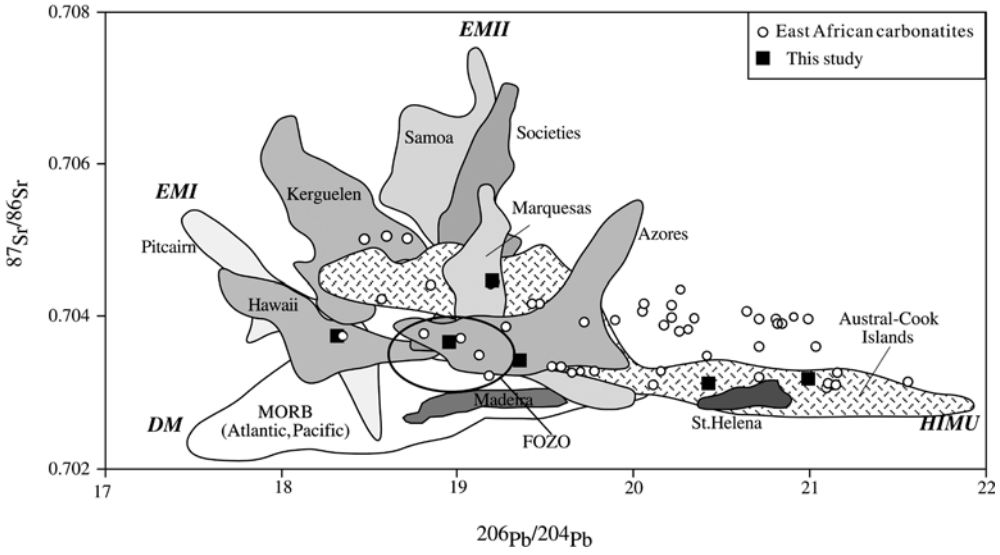

Fig. 12 $^{87}Sr/^{86}Sr$ vs. $^{206}Pb/^{204}Pb$ in East African carbonatites from this study (whole rock data, Table 3) and the literature compared with various OIBs. Carbonatite literature data as in Figs. 4 and 5. Field for the Austral-Cook Island chain from Chauvel et al. (1992, 1997); Hauri and Hart (1993); Nakamura and Tatsumoto (1988); Palacz and Saunders (1986); Vidal et al. (1984). Other OIB and MORB data from Stracke et al. 2003. FOZO field from Hauri et al. (1994). Note that only the Austral Cook Islands have compositions showing mixing between HIMU-EMI mantle components, and that carbonatites with $^{206}Pb/^{204}Pb > 20$ have higher $^{87}Sr/^{86}Sr$ than Austral Cook and St. Helena basalts of the same $^{206}Pb/^{204}Pb$

supported by our observations. The short residence time of the carbonatite source instead, appears in agreement with an asthenospheric origin for these melts (Bell and Tilton 2001) or from a recently metasomatized lithospheric mantle source (Bell and Simonetti 1996).

The initial melts from a lherzolite containing any amount of carbonate will be produced at the carbonated lherzolite solidus, and such melts are carbonatitic (CO_2-rich, Si-poor: Dalton and Presnall 1998; Presnall et al. 2002). If the East African carbonatites are associated with a rising plume (Bell and Tilton 2001) it is conceivable that the volatile-rich (as opposed to the volatile-absent) portions of such an upwelling mantle will preferentially melt upon ascent generating primary carbonatites. However, the available partition coefficients between peridotite and carbonatite melt (Table 6) cannot generate the extreme LREE enrichments and the Hf, Zr and Ti depletions from a normal mantle source without some pre-enrichment process.

Bell and Simonetti (1996) proposed that melts from mantle upwelling beneath East Africa resulted in metasomatism of the subcontinental lithosphere, which melts soon after and produces the carbonatites. In Fig. 13, we present a model that attempts to reconcile an enriched, yet short-lived carbonatitic source, based on experimental constraints and the dynamics of melting within a plume. We assume that primary carbonatitic melts are generated from an ascending mantle plume as it crosses the lherzolite + CO_2 + H_2O solidus. These melts separate from the residue and migrate upwards towards the cooler lithospheric mantle. Some of these melts could erupt directly to the surface depending on their temperature and ascending path (e.g. Lee and Wyllie 2000, path *a* in Fig. 13), while other melts may cool along the shield geotherm, loose heat and freeze *before* they reach the solidus ledge (path *b,* Fig. 13). These melts should precipitate dolomite + silicates along the lherzolite–CO_2 (+ H_2O) solidus (Wyllie 1980). Repetition of this process could create a metasomatic lherzolite with larger carbonate contents than the ambient lithosphere at these depths. This metasomatic horizon will also have high LREE/HREE due to the addition of the small degree carbonatitic melts, along with some Hf, Zr and Ti depletions (if the most extreme $D^{cpx}_{Hf}/D^{cpx}_{Lu}$ ratios are used (Adam and Green 2001); we do note, however, that even higher $D^{cpx}_{Hf}/D^{cpx}_{Lu}$ is required to model the exact depletions). If the local geotherm is subsequently raised (by increased heat supply from the plume either by conductive heating or from subsequent passing melts), then this carbonatite-metasomatized horizon will cross its solidus and melt towards carbonatitic melts (paths *c, c′*, Fig. 13).

The Lu/Hf systematics suggest that the time interval between creation of the new carbonatitic source and melting must be short. This is possible given the anticipated melting dynamics within a rising plume or upwelling mantle. Upwelling mantle plumes are believed to be radially symmetrical with respect to temperature, with the fringes of the plume being cooler than the center (e.g. Ribe and Christensen 1999). As the plume/mantle rises (i.e. beneath the East Africa rift), it crosses its solidus and melts. These first melts are expected to be carbonatitic (since the temperature of the carbonated lherzolite solidus is much lower than the anhydrous solidus; e.g. Presnall et al. 2002), leaving behind a relatively ''dry'' residue. In this sense, a front of very low degree carbonatitic melts is generated ahead of the upwelling mantle and these melts move upwards into the cooler sublithospheric mantle and freeze. As the much hotter center of the plume approaches the area of melt

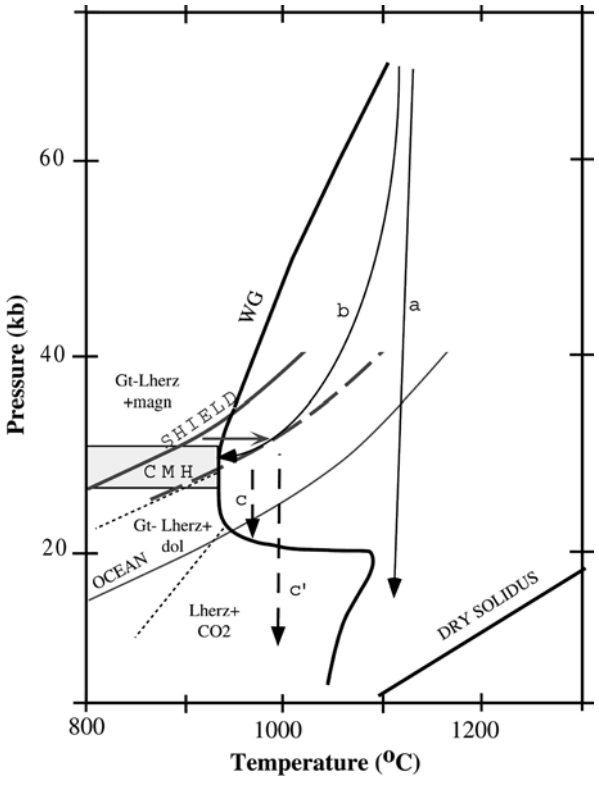

Fig. 13 Schematic model for the generation of a metasomatic carbonatite source. Curve *WG* is the pyrolite + CO_2 + H_2O solidus from Wallace and Green (1988). For pressures higher than 32 kb, we assume that the solidus continues with the same slope as the solidus in the CMAS–CO_2 system determined by Dalton and Presnall 1998. *SHIELD* and *OCEAN* geotherms from Fallon and Green (1990). The continuation of these curves at depth is uncertain but that does not affect our modeling. *DRY SOLIDUS* curve (Fallon and Green 1990) is shown for comparison. *Dotted lines* define the subsolidus mineral assemblages (Fallon and Green 1990; Wallace and Green 1988). *Shaded rectangle CMH* denotes the carbonatite-metasomatized-horizon of our model. *Arrows a* and *b,* denote the paths of carbonatite melts generated within an ascending mantle plume. *Path a* shows a carbonatite melt generated at depth that erupts directly towards the surface (similar to path 1 of Lee and Wyllie 2000). *Path b* shows a carbonatitic melt that loses heat as it ascends and crystallizes at pressure greater than 22 kb, creating the CMH body. If the local geotherm is raised (*horizontal arrow* from the *SHIELD* geotherm to its parallel *dashed line*) *CMH* will melt generating carbonatitic melts *C, C′*. These may react at the solidus ledge (*path C*, Green and Wallace 1988; Dalton and Wood 1993), or continue through crack propagation to the surface (*path C′*, Lee and Wyllie 2000)

generation, higher degree alkali-silicate melts are produced. These melts could erupt directly to the surface, possibly along conduits created by the earlier carbonatitic melts. Any previously created carbonatite metasomatized horizon along the path of these later melts will be consumed by the silicate melts. However, the rise of the silicate melts and the approaching hot center of the plume will heat up *adjacent* carbonatite-metasomatized horizons (i.e. not along the path of the silicate melts). This will raise the local geotherm generating melting and eruption of carbonatites, *after* the silicate eruption. In a sense then, carbonatite melts are generated first but because of the presence of the cooler continental lithosphere they erupt last, as it is frequently observed in carbonatite complexes (Barker 1989; Harmer and Gittins 1998). This model is consistent with the occurrence of carbonatite–nephelinite centers (including Bukusu and Sukulu) marginal to the present-day location of the Kenya Dome (at the Kenya Rift Zone) which, in turn, is dominated by basalt/phonolite lavas (e.g. Bell and Simonetti 1996). This model is also compatible with the rarity of carbonatites in the oceanic lithosphere: the oceanic geotherm will cross the lherzolite + CO_2 solidus much closer to the solidus ledge (Fig. 13) thereby preventing the deep carbonatitic melts from freezing along the carbonated peridotite solidus and forcing them to react with orthopyroxene through the solidus ledge towards the decarbonation reaction and release of volatiles (e.g. Green and Wallace 1988).

Our model is rather qualitative, and it depends on the intersection of the geotherm and the solidus of the carbonated-lherzolite, which in turn depends in the presence or absence of H_2O and the oxidation conditions in the mantle (Falloon and Green 1990). For example, in the absence of H_2O, the carbonated lherzolite solidus will shift to higher temperature (about 100 °C higher; Fallon and Green 1990), while retaining the characteristic solidus ledge. This will shift the geotherm/solidus intersection to higher pressures and temperatures, essentially increasing the area above the solidus ledge where the first carbonatitic melts can freeze. The generation of a metasomatic source for the erupting carbonatites is also compatible with their HIMU-EMI (+EMII?) isotope characteristics because it provides an additional component, other than the plume, in their source. However, the present data cannot resolve where the EM (I, II) and HIMU endmembers actually reside (i.e. plume or lithosphere; Bell and Simonetti 1996).

Conclusions

A detailed investigation of the trace element distribution in carbonatites reveals that the whole rock Nd (REE) and Sr elemental budget is dominated by the carbonate fraction while Hf, Zr and Ti primarily reside in the non-carbonate fraction of these rocks. The combined Nd, Sr and Hf isotope investigation shows frequent isotopic disequilibrium between the carbonate and non-carbonate fractions. The isotopic disequilibrium rules out the origin of the non-carbonates as products of immiscibility/or crystal fractionation from an evolving carbonatitic magma. Instead, they must represent xenocrysts picked up by the carbonatite magma en route to the surface. Since the carbonate fraction dominates the volume and most of the trace element budget we suggest that the carbonate and not the whole rock better reflects the isotopic composition of the carbonatitic magma and in turn the composition of the carbonatite source. Based on available experimental partitioning data, it is suggested that the carbonatite source will have equal or higher Lu/

Hf ratio than the carbonatite. Such a carbonatite source can only exist for a very short time period in the mantle or even crust (ca. 10–50 Ma), otherwise it would develop extremely radiogenic Hf compositions which are not observed in carbonatites or any other terrestrial magmas. Irrespective of its exact Hf isotopic composition, the carbonatite source either has to melt out soon after its formation or mix efficiently back into the mantle. We present a model where a carbonatite source is generated in the lithospheric mantle from the first carbonatitic melts rising from an ascending mantle plume. These melts freeze at higher levels in the cooler lithosphere generating a carbonatite metasomatized horizon. As the much hotter center of the plume approaches, the excess heat from the plume and/or the subsequent rising silicate melts will raise the geotherm, thereby inducing melting in the metasomatic horizon and generation of the carbonatite melts that are observed on the surface. This model can explain the strong enrichments in trace elements in carbonatites, their HIMU-EMI (+EMII) isotope characteristics and the rarity of carbonatites in the oceanic lithosphere. Ours is the first detailed study of the Hf isotopes in carbonatites and further Hf isotope investigations may reveal whether longer-lived carbonatite sources do exist. Targeted studies should include the silicate rocks within the carbonatitic complexes (nephelinites, phonolites etc.) in order to investigate the relationship of the carbonatites to these silicate rocks, perhaps resolving the opposing theories of liquid immiscibility and fractionation versus distinct magmas for the origin of these intimately-related rock types.

Acknowledgements The carbonatite samples for this study were collected by J.B.D. when a member of the Tanganyika Geological Survey and during a visit to Uganda, Malawi and South Africa funded by the Institute of Mining and Metallurgy. Keith Bell and an anonymous reviewer are thanked for their in-depth reviews that greatly improved the manuscript. A. Stracke and G. Sen are thanked for their comments. Funding for this project was provided by NSF grants EAR 0124961 and EAR 952669 to V. Salters. The manuscript preparation was funded by NSF grant OCE 9810961 to Gautam Sen (Florida International University).

Appendix

All trace element concentrations (except were noted by isotope dilution) were determined at NHMFL using a Finnigan MAT ELEMENT 1, high resolution ICP-MS, with a CD1E interface. For sample introduction we used a Cetac MCN 6000 desolvating nebulizer with a 50 µl Teflon nebulizer in self-aspiration mode and Teflon tubing. The enhanced instrument sensitivity with this configuration allows the introduction of low total dissolved solid content in the instrument (100 ppm), which minimizes matrix-related drift and signal instabilities. A mixture of nitrogen and argon was used as sample gas in order to minimize oxide interference, which in the case of carbonatites can be significant on the middle and heavy REE and Hf, due to the high LREE/HREE and Ba/HREE ratios and in the case of Hf, high Dy/Hf ratios in carbonatites. The oxide formation of these elements varies monotonically with the Th oxide formation (ThO^+/Th^+) which was kept at less than 0.06% by adjusting the Ar/N ratio in the sample gas, while keeping signal intensity at optimum conditions. At these levels of Th oxide formation, the other interfering oxides resulted in negligible corrections to the measured elements (e.g. $^{162}Dy^{16}O/^{162}Dy < 0.001\%$, resulting in negligible corrections at ^{178}Hf).

The sample powders were dissolved in HF/HNO_3 mixture for at least 48 h, dried and redissolved in 2% HNO_3 at 100 ppm total dissolved solid content. For external standard we used the reference material BHVO-1 (Kilauea basalt) with the concentrations reported by Eggins et al. (1997). Measurement sequences were less than 1 h long and consisted of procedural blank, standard, two unknowns and the standard. Indium (at 1 ppb concentration) was used as an internal spike in all samples to monitor and correct for signal drift during measurement. The concentrations for each element were calculated by combining linear interpolation between the bracketing standards and normalizing concentrations to the ^{115}In intensity for each sample. Reproducibility was determined by repeated measurements of the COQ sample and it was 5% or better for all elements.

The Hf, Zr and Ti depletions (Table 2) are defined here as follows: $Hf/Hf^* = (Hf_C/Hf_{Chon})/(Nd_C/Nd_{Chon}*1/3 + Sm_C/Sm_{chon}*2/3)$, $\cdot\ Zr/Zr^* = (Zr_C/Zr_{Chon})/(Nd_C/Nd_{Chon}*2/3 + Sm_C/Sm_{chon}*1/3)$, $\cdot\ Ti/Ti^* = (Ti_C/Ti_{Chon})/(Eu_C/Eu_{Chon}*1/2 + Gd_C/Gd_{chon}*1/2)$, where subscript C denotes concentration in the sample and *chon* chondrite concentration.

Nd, Sr and Pb chemical separations were carried out at NHMFL using previously established techniques (Hart and Brooks 1977; Manhès et al. 1978; Richard et al. 1976; Zindler et al. 1979). Nd, Sr and Pb isotope determinations were performed at NHMFL using a FINNIGAN MAT 262 RPQ mass spectrometer. Nd and Sr isotopic determinations were performed with a multi-collector dynamic routine. Pb isotope compositions were measured in the static mode using fully automated temperature control at 1,250 °C (see footnotes in Table 3 for further details).

The Hf chemical separation employed here is modified after the method of Salters (1994). The use of concentrated HF during dissolution coupled with the high Ca contents of carbonatites and the large amounts of required sample resulted in very low Hf yields due to the co-precipitation of Hf with insoluble CaF_2. To efficiently separate Hf from Ca, we employed a double-dissolution technique: the carbonate fraction was first dissolved and separated from the silicate fraction using either $HCl:HNO_3$ mixture or hot 2.5 N HCl and the remaining silicate fraction (always less than 20 mg) was dissolved in hot $HF:HNO_3$ mixture (3:1) and converted to 2.5 N HCl. This technique resulted in clear solutions with no obvious undissolved material for both the carbonate and silicate fractions, which were then combined into one

solution containing the whole rock in 2.5 N HCl. If any residue was present in any of the two solutions, the sample was aborted and the dissolution was repeated. Hf, Zr, Ti (along with some Al, Fe, and Mg) was separated from the rest of the matrix using all-Teflon columns filled with cation resin in 4 ml 2.5 N HCl/0.1 N HF acid. At this acid normality and despite the presence of fluorides, Sr and the REE remain in the column and can be subsequently mobilized in the same fashion as in the typical cation exchange techniques. This technique allows the efficient separation of Hf from Ca (critical for the following separation steps that require HF) and the quantitative recovery of Sr and the REE for Sr and Nd isotope determination. This column chemistry was employed for the determination of the Hf, Sr and Nd isotopic compositions of the silicate fractions from a single dissolution. The Hf cut from the cation columns was further purified following the method of Salters (1994). To verify the reproducibility of this double-dissolution technique, we also processed sample BD 1584 with the original method of Salters (1994) (whole rock HF dissolution: this was the only sample we could process this way because of its higher Hf contents). The measured $^{176}Hf/^{177}Hf$ ratio was identical within error for both methods (Table 5: *BD 1584 wr* and *wr duplicate*, respectively). For the Hf isotope determination of the carbonate fractions (which required at least 3 g of sample), we used larger cation columns (14-ml cation resin) in order to increase the amount of Ca retained in the column. Hf blanks where less than 10 pg, and less than 20 pg when the large cation columns where used.

The Lu/Hf ratios of the carbonate fractions were determined by isotope dilution. A fraction of the dissolved carbonate was spiked with ^{175}Lu and ^{179}Hf, and dried. The Lu/Yb fraction was collected from the cation columns and Lu was further purified from Yb using columns packed with HDEHP-coated teflon powder and eluted with 4 N HCl. Lu was measured on the 262 MAT Finnigan using the double Re filament technique. The reproducibility of the Lu/Hf ratio was determined by repeated measurements of the BIR-1 basalt standard: $Lu/Hf = 0.06102 \pm 0.00033$ (1 SD, $n = 3$).

All Hf isotope compositions were determined at NHMFL with the Lamont ISOLAB (England et al. 1992) using the hot SIMS technique (Salters 1994). The external reproducibility of the instrument over a 2-year period was determined by repeated measurements of the standard JMC-475: $^{176}Hf/^{177}Hf = 0.282200 \pm 31$ (2 SD, $n = 44$) which is in excellent agreement with the reported value before the instrument was relocated to NHMFL from LDEO (Salters 1994). Because of the variable amounts of Hf present in carbonatites, the JMC-475 reproducibility was determined by loading variable amounts of Hf (50–150 ng). If only the larger loads are considered (110–150 ng), the reproducibility improves but the average value remains essentially identical: $^{176}Hf/^{177}Hf = 0.282199 \pm 24$ (2 SD, $n = 13$). $^{176}Hf/^{177}Hf$ ratios were fractionation corrected using $^{177}Hf/^{178}Hf = 0.6816$. All Hf isotope compositions are reported relative to the value of 0.282160 for the JMC standard.

References

Adam J, Green T (2001) Experimentally determined partition coefficients for minor and trace elements in peridotite minerals and carbonatitic melt, and their relevance to natural carbonatites. Eur J Mineral 13:815–827

Anders E, Grevesse N (1989) Abundances of the elements: meteoritic and solar. Geochim Cosmochim Acta 53:197–214

Bailey DK (1993) Carbonate magmas. J. Geol. Soc. London 150:637–651

Barker D (1989) Field relations of carbonatites. In: Bell K (ed) Carbonatites: genesis and evolution. Unwin Hyman, London, pp 38–69

Barker D (1996) Carbonatite volcanism. In: Mitchell RH (ed) Undersaturated alkaline rocks: mineralogy, petrogenesis, and economic potential, vol 24. Mineralogical Association of Canada, Winnipeg, Manitoba, pp 45–61

Barker DS, Nixon PH (1989) High-Ca, low-alkali carbonatite volcanism at Fort Portal, Uganda. Contrib Mineral Petrol 103:166–177

Bell K (1998) Radiogenic isotope constraints on relationships between carbonatites and associated silicate rocks—a brief review. J Petrol 39:1987–1996

Bell K, Blenkinsop J (1987) Nd and Sr isotopic compositions of East African carbonatites: implications for mantle heterogeneity. Geology 15:99–102

Bell K, Blenkinsop J (1989) Neodymium and strontium isotope geochemistry of carbonatites. In: Bell K (ed) Carbonatites—genesis and evolution. Unwin Hyman, Boston, pp 278–300

Bell K, Kjarsgaard BA, Simonetti A (1998) Carbonatites—into the twenty-first century. J Petrol 39:1839–1845

Bell K, Simonetti A (1996) Carbonatite magmatism and plume activity: implications from the Nd, Pb and Sr isotope systematics of Oldoinyo Lengai. J Petrol 37:1321–1339

Bell K, Tilton GR (2001) Nd, Pb and Sr isotopic compositions of East African Rift carbonatites: evidence for mantle mixing and plume heterogeneity. J Petrol 42:1927–1945

Blundy J, Dalton J (2000) Experimental composition of trace element partitioning between clinopyroxene and melt in carbonate and silicate systems, implications for mantle metasomatism. Contrib Mineral Petrol 139:356–371

Brooker RA (1998) The effect of CO_2 saturation on immiscibility between silicate and carbonate liquids: an experimental study. J Petrol 39:1905–1915

Chauvel C, Hofmann AW, Vidal P (1992) HIMU- EM: the French Polynesia connection. Earth Planet Sci Lett 110:99–119

Chauvel C, McDonough W, Guille W, Maury R, Duncan R (1997) Contrasting old and young volcanism in Rurutu Island, Austral chain. Chem Geol 139:125–143

Church AA, Jones AP (1995) Silicate-carbonate immiscibility at Oldoinyo Lengai. J Petrol 36:869–889

Coltorti M, Bonadiman C, Hinton RW, Siena F, Upton BG J. (1999) Carbonatite metasomatism of the oceanic upper mantle: evidence from clinopyroxenes and glasses in ultramafic xenoliths of Grande Comore, Indian Ocean. J Petrol 40:133–165

Dalton JA, Presnall DC (1998) The continuum of primary carbonatitic-kimberlitic melt compositions in equilibrium with lherzolite: data from the system $CaO–MgO–Al_2O_3–SiO_2–CO_2$ at 6 GPa. J Petrol 39:1953–1964

Dalton JA, Wood BJ (1993) The compositions of primary carbonate melts and their evolution through wallrock reaction in the mantle. Earth Planet Sci Lett 119:511–525

Dawson JB (1987) Metasomatized harzburgites in kimberlites and alkaline magmas: enriched restites and 'flushed' lherzolites. In:

Hawkesworth CJ, Menzies MA (eds) Mantle metasomatism. Academic Press, London, pp 125–144
Dawson JB, Powell DG, Reid AM (1970) Ultrabasic xenoliths and lava from the Lashaine volcano, northern Tanzania. J Petrol 11:519–548
Dawson JB, Pinkerton H, Pyle DM, Nyamweru C (1994) June 1993 eruption of Oldoinyo Lengai, Tanzania: exceptionally viscous and large carbonatite lava flows and evidence for coexisting silicate and carbonatite magmas. Geology 22:799–802
Dawson JB, Pinkerton H, Norton GE, Pyle DM, Browning P, Jackson D, Fallick AE (1995) Petrology and geochemistry of Oldoinyo Lengai lavas extruded in November 1988: magma source, ascent and crystallization. In: Bell K, Keller J (eds) Carbonatite volcanism. Springer, Berlin Heidelberg New York, pp 47–69
Dawson JB, Steele IM, Smith JV, Rivers ML (1996) Minor and trace element chemistry of carbonates, apatites and magnetites in some African carbonatites. Mineral Mag 60:415–425
Dupuy C, Liotard JM, Dostal J (1992) Zr/Hf fractionation in intraplate basaltic rocks: carbonate metasomatism in the mantle source. Geochim Cosmochim Acta 56:2417–2423
Eggins SM, Woodhead JD, Kinsley LPJ, Mortimer GE, Sylvester P, McCulloch MT, Hergt JM, Handler MR (1997) A simple method for the precise determination of >40 trace elements in geological samples by ICPMS using enriched isotope internal standards. Chem Geol 134:311–326
England JG, Zindler A, Reisberg LC, Rubenstone JL, Salters V, Marcantonio F, Bourdon B, Brueckner H, Turner PJ, Weaver S, Read P (1992) The Lamont Doherty Geological Observatory ISOLAB 54 isotope ratio mass spectrometer. Int J Mass Spec Ion Proc 121:201–240
Fallon TJ, Green DH (1990) Solidus of carbonated fertile peridotite under fluid-saturated conditions. Geology 18:198–199
Foley SF, Barth MG, Jenner GA (2000) Rutile/melt partition coefficients for trace elements and an assessment of the influence of rutile on the trace element characteristics of subduction zone magmas. Geochim Cosmochim Acta 64:933–938
Garson MS (1962) The Tundulu carbonatite ring complex in southern Nyasaland. Memoir 2, Geol Survey Nuasaland
Green DH, Wallace ME (1988) Mantle metasomatism by ephemeral carbonatite melts. Nature 336:459–461
Green TH, Adam J, Sie SH (1992) Trace element partitioning between silicate minerals and carbonatite at 25 kbar and application to mantle metasomatism. Mineral Petrol 46:179–184
Grünenfelder MH, Tilton GR, Bell K, Blenkinsop J (1986) Lead and strontium isotope relationships in the Oka carbonatite complex, Quebec. Geochim Cosmochim Acta 50:461–468
Hamilton DL, Bedson P, Esson J (1989) The behaviour of trace elements in the evolution of carbonatites. In: Bell K (ed) Carbonatities: genesis and evolution. Unwin Hyman, Boston, pp 405–427
Hanan BB, Graham, DW (1996) Lead and helium isotope evidence from oceanic basalts for a common deep source of mantle plumes. Science 272: 991–995
Harmer RE (1985) A Sr isotope study of Transvaal carbonatites. Trans Geol Soc S Afr 88:471–477
Harmer RE (1999) The petrogenetic association of Carbonatite and Alkaline Magmatism: constraints from the Spitskop complex, South Africa. J Petrol 40: 525–548
Harmer RE, Gittins J (1997) The origin of dolomitic carbonatites: Field and experimental constraints. J Afr Earth Sci 25:5-28
Harmer RE, Gittins J (1998) The case for primary, mantle-derived carbonatite magma. J Petrol 39:1895–1903
Hart SR, Brooks C (1977) The geochemistry and evolution of the early Precambrian mantle. Contrib Mineral Petrol 61:109–128
Hart SR, Hauri EH, Oschmann LA, Whitehead JA (1992) Mantle plumes and entrainment: Isotopic evidence. Science 256:517–520
Hauri EH, Hart SR (1993) Re-Os isotope systematics of HIMU and EMII oceanic island basalts from the South Pacific Ocean. Earth Planet. Sci. Lett. 114:353–371
Hauri E, Shimizu N, Dieu J, Hart SR (1993) Evidence for hotspot-related carbonatite metasomatism in the oceanic upper mantle. Nature 365:221–227
Hogarth DD (1989) Pyrochlore, apatite, and amphibole: distinctive minerals in carbonatite. In: Bell K (ed) Carbonatites—genesis and evolution. Unwin Hyman, Boston, pp 105–148
Hornig-Kjarsgaard I (1998) Rare earth elements in sovitic carbonatites and their mineral phases. J Petrol 39:2105–2121
Ionov D (1998) Trace element composition of mantle-derived carbonates and coexisting phases in peridotite xenoliths from alkali basalts. J Petrol 39:1931–1941
Ionov D, Harmer R (2002) Trace element distribution in calcite-dolomite carbonatites from Spitskop: inferences for differentiation of carbonatite magmas and the origin of carbonates in mantle xenoliths. Earth Planet Sci Lett 198:495–510
Kalt A, Hegner E, Satir M (1997) Nd, Sr, and Pb isotopic evidence for diverse lithospheric mantle sources of East African Rift carbonatites. Tectonophysics 278:31–45
Kato T, Ringwood AE, Irifune T (1988) Constraints on element partition coefficients between $MgSiO_3$ perovskite and liquid determined by direct measurements. Earth Planet Sci Lett 90:65–68
Kjarsgaard BA (1998) Phase relations of a carbonated high-CaO nephelinite at 0.2 and 0.5 GPa. J Petrol 39:2061–2075
Klemme S, van der Laan SR, Foley SF, Gunther D (1995) Experimentally determined trace and minor element partitioning between clinopyroxene and carbonatite melt under upper mantle conditions. Earth Planet Sci Lett 133:439–448
Kuehner SM, Laughlin JR, Grossman L, Johnson ML, Burnett DS (1989) Determination of trace element mineral/liquid partition coefficients in melilite and diopside by ion and electron microprobe techniques. Geochim Cosmochim Acta 53:3115–3130
Larsen (1979) Distribution of REE and other trace elements between phenocrysts and peralkaline undersaturated magmas, exemplified by rocks from the Gardar igneous province, south Greenland. Lithos 12:303–315
Lee C-T, Rudnick RL, McDonough W, Horn I (2000) Petrologic and geochemical investigation of carbonates in peridotite xenoliths from northeastern Tanzania. Contrib Mineral Petrol 139:470–484
Lee W, Wyllie PJ (1997a) Liquid immiscibility between nephelinite and carbonatite from 1.0 to 2.5 GPa compared with mantle melt compositions. Contrib Mineral Petrol 127:1–16
Lee W, Wyllie PJ (1997b) Liquid immiscibility in the join of $NaAlSiO_4$–$NaAlSi_3O_8$–$CaCO_3$ at 1 GPa: implications for crustal carbonatites. J Petrol 38:1113–1135
Lee WL, Wyllie PJ (2000) The system CaO-MgO-SiO_2-CO_2 at 1 GPa, metasomatic wehrlites, and primary carbonatite magmas. Contrib Min Petrol 138:214–228
Lee WJ, Huang WL, Wyllie P (2000) Melts in the mantle modeled on the system CaO-MgO-SiO_2-CO_2 at 2.7 GPa. Contrib Mineral Petrol 138:199–213
Manhès G, Minster J-P, Allègre CJ (1978) Comparative uranium-thorium-lead and rubidium-strontium of St. Severin amphoterite: consequences for early solar system chronology. Earth Planet Sci Lett 39:14–24
McDonough WF, Sun S-S (1995) The composition of the Earth. Chem Geol 120:223–253
Moore KR, Wood BJ (1998) The transition from carbonate to silicate melts in the CaO–MgO–SiO_2–CO_2 system. J Petrol 39:1943–1951
Nakamura Y, Tatsumoto M (1988) Pb, Nd, and Sr isotopic evidence for a multicomponent source for rocks of Cook-Austral Islands and heterogeneities of mantle plumes. Geochim Cosmochim Acta 52:2909–2924
Nelson DR, Chivas AR, Chappell BW, McCulloch MT (1988) Geochemical and isotopic systematics in carbonatites and implications for the evolution of ocean-island sources. Geochim Cosmochim Acta 52:1–17
Palacz ZA, Saunders AD (1986) Coupled trace element and isotope enrichment in the Cook-Austral-Samoa islands, southwest Pacific. Earth Planet Sci Lett 79:270–280

Paslick C, Halliday A, James D, Dawson JB (1995) Enrichment of the continental lithosphere by OIB melts: isotopic evidence from the volcanic province of northern Tanzania. Earth Planet Sci Lett 130:109–126

Petibon CM, Kjarsgaard BA, Jenner GA, Jackson SE (1998) Phase relationships of a silicate-bearing natrocarbonatite from Oldoynio Lengai at 20 and 100 MPa. J Petrol 39:2137–2151

Presnall DC, Gudfinnsson GH, Walter MJ (2002) Generation of mid-ocean ridge basalts at pressures from 1 to 7 GPa. Geochim Cosmochim Acta 66:2073–2090

Ribe NM, Christensen UR (1999) The dynamical origin of Hawaiian volcanism. Earth Planet Sci Lett 171:517–531

Richard PN, Shimizu N, Allègre CJ (1976) $^{143}Nd/^{144}Nd$, a natural tracer: an application to oceanic basalts. Earth Planet Sci Lett 31:269–278

Rudnick RL, McDonough F, Chappell BW (1993) Carbonatite metasomatism in the northern Tanzanian mantle: petrographic and geochemical characteristics. Earth Planet Sci Lett 114:463–475

Salters VJM (1994) $^{176}Hf/^{177}Hf$ determination in small samples by a high temperature SIMS technique. Anal Chem 66:4186–4189

Salters VJM, Longhi J (1999) Trace element partitioning during the initial stages of melting beneath mid-ocean ridges. Earth Planet Sci Lett 166:15–30

Salters VJM, Shimizu N (1988) World-wide occurrence of HFSE-depleted mantle. Geochim Cosmochim Acta 52: 2177–2182

Salters VJM, White WM (1998) Hf isotope constraints on mantle evolution. Chem Geol 145:447–460

Salters VJM, Longhi J, Bizimis M (2002) Near mantle solidus trace element partitioning at pressures up to 3.4 GPa. Geochem Geophys Geosyst 2001GC000173

Schleicher H, Keller J, Kramm U (1990) Isotope studies on alkaline volcanics and carbonatites from the Kaiserstuhl, Federal Republic of Germany. Lithos 26:21–35

Seifert W, Kampf H, Wasternack J (2000) Compositional variation in apatite, phlogopite and other accessory minerals of the Delitzsch complex, Germany: implication for cooling history of carbonatites. Lithos 53:81–100

Simonetti A, Bell K (1994) Isotopic and geochemical investigation of the Chilwa Island Carbonatite Complex, Malawi: evidence for a depleted mantle source region, liquid immiscibility, and open system melting. J Petrol 35:1597–1621

Simonetti A, Bell K, Shrady C (1997) Trace- and rare-earth-element geochemistry of the June 1993 natrocarbonatite lavas, Oldoinyo Lengai (Tanzania): implications for the origin of carbonatite magmas. J Volcan Geotherm Res 75:89–106

Stracke A, Bizimis M, Salters VJM (2003) Recycling oceanic crust: Quantitative constraints. Geochem Geophys Geosyst 2001GC000223

Sweeney RJ, Green DH, Sie SH (1992) Trace and minor element partitioning between garnet and amphibole and carbonatitic melt. Earth Planet Sci Lett 113: 1–14

Sweeney RJ, Prozesky V, Przylowicz W (1995) Selected trace and minor element partitioning between peridotite minerals and carbonatite melts at 18–46 kb pressure. Geochim Cosmochim Acta 59:3671–3683

Todt W, Cliff RA, Hanser A, Hofmann AW (1996) Evaluation of a $^{202}Pb + ^{205}Pb$ double spike for high precision lead isotope analyses. In: Basu A, Hart S (eds) Earth processes: reading the isotopic code, vol 95. American Geophysical Union, pp 429–437

Van Straaten P (1989) Nature and structural relationships of carbonatites from Southwest and West Tanzania. In: Bell K (ed) Carbonatites—genesis and evolution. Unwin Hyman, Boston, pp. 177–199

Veksler IV, Petibon C, Jenner GA, Dorfman AM, Dingwell DB (1998) Trace element partitioning in immiscible silicate-carbonate liquid systems: an initial experimental study using a centrifuge autoclave. J Petrol 39:2095–2104

Verwoerd (1967) The carbonatites of South Africa and South West Africa. Handb 6 Geol Soc S Africa. 452p

Vervoort JD, Patchett JP, Blichert-Toft J, Albarede F (1999) Relationships between Lu-Hf and Sm–Nd isotopic systems in the global sedimentary system. Earth Planet Sci Lett 168:79–99

Vidal P, Chaucel C, Brousse R (1984) Large mantle heterogeneity beneath French Polynesia. Nature 307:536–538

Wallace ME, Green DH (1988) An experimental determination of primary carbonatite magma composition. Nature 335: 343–346

Wen J, Bell K, Blenkinshop J (1987) Nd and Sr isotope systematics of the Oka complex, Quebec, and bearing on the evolution of the subcontinental upper mantle. Contrib Mineral Petrol 97:433–437

Woolley AR (1989) The spatial and temporal distribution of carbonatites. In: Bell K (ed) Carbonatites: nomenclature, average chemical composition. Unwin Hyman, Boston

Woolley AR (2001) Alkaline rocks and carbonatites of the world. Part 3: Africa. Geol Soc, London

Woolley AR, Jones GC (1987) The petrochemistry of the northern part of the Chilwa alkaline province, Malawi. In: Fitton JG, Upton BJG (eds) Alkaline igneous rocks. vol 30. Geol Soc, Spec Publ, pp 335–355

Woolley AR, Kempe DRC (1989) Carbonatites: nomenclature, average chemical composition. In: Bell K (ed) Carbonatities: genesis and evolution. Unwin Hyman, Boston, pp 1–14

Wyllie PJ (1980) The origin of kimberlite. J Geophys Res 85: 6902–7010

Wyllie PJ, Huang W-L (1975) Peridotite, kimberlite, and carbonatite explained in the system $CaO–MgO–SiO_2–CO_2$. Geology 3:621–624

Wyllie PJ, Lee WJ (1998) Model system controls on conditions for formation of magnesiocarbonatite and calsiocarbonatite magmas from the mantle. J Petrol 39:1883–1893

Yaxley GM, Crawford AJ, Green DH (1991) Evidence for carbonatite metasomatism in spinel peridotite xenoliths from western Victoria, Australia. Earth Planet Sci Lett 107: 305–317

Yaxley GM, Green DH, Kamenetsky V (1998) Carbonatite metasomatism in the southeastern Australian lithosphere. J Petrol 39:1917–1930

Zindler A, Hart SR (1986) Chemical Geodynamics. Annu Rev Earth Planet Sci 14:493–571

Zindler A, Hart SR, Frey FA, Jakobsson SP (1979) Nd and Sr isotope ratios and rare earth element abundances in Reykjanes peninsula basalts: evidence for mantle heterogeneity beneath Iceland. Earth Planet Sci Lett 45:249–262